



Calhoun: The NPS Institutional Archive
DSpace Repository

Theses and Dissertations

1. Thesis and Dissertation Collection, all items

1982-06

Atmospheric effects on ultra high frequency radio propagation

Boudreaux, Joseph Clent

Monterey, California. Naval Postgraduate School

<http://hdl.handle.net/10945/20082>

Downloaded from NPS Archive: Calhoun



<http://www.nps.edu/library>

Calhoun is the Naval Postgraduate School's public access digital repository for research materials and institutional publications created by the NPS community. Calhoun is named for Professor of Mathematics Guy K. Calhoun, NPS's first appointed -- and published -- scholarly author.

Dudley Knox Library / Naval Postgraduate School
411 Dyer Road / 1 University Circle
Monterey, California USA 93943

LEY KNOX LIBRARY
POSTGRADUATE SCHOOL
TEREY, CALIF. 93940

NAVAL POSTGRADUATE SCHOOL

Monterey, California



THESIS

ATMOSPHERIC EFFECTS ON
ULTRA HIGH FREQUENCY RADIO PROPAGATION

by

Joseph Clent Boudreaux, III

June 1982

Thesis Advisor:

G. E. Schacher

Approved for public release; distribution unlimited

T204553

REPORT DOCUMENTATION PAGE		READ INSTRUCTIONS BEFORE COMPLETING FORM
1. REPORT NUMBER	2. GOVT ACCESSION NO.	3. RECIPIENT'S CATALOG NUMBER
4. TITLE (and Subtitle) ATMOSPHERIC EFFECTS ON ULTRA HIGH FREQUENCY RADIO PROPAGATION		5. TYPE OF REPORT & PERIOD COVERED Master's Thesis; June 1982
		6. PERFORMING ORG. REPORT NUMBER
7. AUTHOR(s) Joseph Clent Boudreaux, III		8. CONTRACT OR GRANT NUMBER(s)
9. PERFORMING ORGANIZATION NAME AND ADDRESS Naval Postgraduate School Monterey, California 93940		10. PROGRAM ELEMENT, PROJECT, TASK AREA & WORK UNIT NUMBERS
11. CONTROLLING OFFICE NAME AND ADDRESS Naval Postgraduate School Monterey, California 93940		12. REPORT DATE June 1982
		13. NUMBER OF PAGES 87
14. MONITORING AGENCY NAME & ADDRESS (if different from Controlling Office)		15. SECURITY CLASS. (of this report)
		15a. DECLASSIFICATION/DOWNGRADING SCHEDULE
16. DISTRIBUTION STATEMENT (of this Report) Approved for public release; distribution unlimited		
17. DISTRIBUTION STATEMENT (of the abstract entered in Block 20, if different from Report)		
18. SUPPLEMENTARY NOTES		
19. KEY WORDS (Continue on reverse side if necessary and identify by block number) electromagnetic propagation, atmospheric propagation, atmospheric refractive ducting, ducting, diffraction, multimode waveguide, ray tracing, mode theory		
20. ABSTRACT (Continue on reverse side if necessary and identify by block number) The dependence of received power on range within and below atmospheric ducts was measured in conditions of elevated, nonhomogeneous, multilayered ducts. An aircraft with UHF transmitter covered the range 0 to 150 nm. from a shore based receiver. Range dependent maxima and minima in received power were detected at the surface in elevated duct conditions. The results were compared to predictions from		

20. (Continued)

ray, waveguide multi-mode, and single mode theories. Ray and single mode theories were inadequate to predict power patterns over the horizon. Multi-mode theory yielded qualitative agreement for conditions of deep, low elevated ducts. Agreement for higher, thinner ducts was poor. Multilayered duct systems were observed and produced interference patterns without recognizable period with range.

Approved for public release; distribution unlimited.

Atmospheric Effects on
Ultra High Frequency Radio Propagation

by

Joseph Clent Boudreaux, III
Lieutenant Commander, United States Navy
B.S., United States Naval Academy, 1969

Submitted in partial fulfillment of the
requirements for the degree of

MASTER OF SCIENCE IN PHYSICS

from the

NAVAL POST GRADUATE SCHOOL

June 1982

137335
S11

ABSTRACT

The dependence of received power on range within and below atmospheric ducts was measured in conditions of elevated, nonhomogeneous, multilayered ducts. An aircraft with UHF transmitter covered the range 0 to 150 nm. from a shore based receiver. Range dependent maxima and minima in received power were detected at the surface in elevated duct conditions. The results were compared to predictions from ray, waveguide multi-mode, and single mode theories. Ray and single mode theories were inadequate to predict power patterns over the horizon. Multi-mode theory yielded qualitative agreement for conditions of deep, low elevated ducts. Agreement for higher, thinner ducts was poor. Multilayered duct systems were observed and produced interference patterns without recognizable period with range.

TABLE OF CONTENTS

I.	INTRODUCTION -----	10
II.	EXPERIMENTAL PROCEDURE -----	12
A.	EQUIPMENT -----	12
1.	AIRCRAFT -----	12
2.	RECEIVER SITE -----	13
B.	CALIBRATION -----	14
1.	RECEIVER SYSTEM -----	14
2.	TRANSMITTER SYSTEM -----	16
3.	COAXIAL CABLES -----	19
C.	METHOD -----	20
1.	GENERAL -----	20
2.	FLIGHT PATHS -----	20
3.	FLIGHT PROFILES -----	23
4.	AIRCRAFT PROCEDURES -----	25
5.	RECEIVER SITE PROCEDURES -----	26
D.	DATA ANALYSIS -----	27
1.	GENERAL -----	27
2.	LOSS CURVES -----	27
3.	M PROFILES -----	29
4.	HEIGHT GAIN CURVES -----	30
III.	THEORY -----	31
A.	GENERAL -----	31
B.	RAY THEORY -----	31
C.	MODE THEORY -----	36

D. SINGLE MODE APPROXIMATION -----	41
IV. EXPERIMENTAL RESULTS -----	44
A. GENERAL -----	44
B. M PROFILES -----	44
C. HEIGHT GAIN CURVES -----	45
D. LOSS CURVES -----	50
1. AIRCRAFT BELOW THE DUCT -----	50
2. AIRCRAFT IN THE DUCT -----	52
V. CONCLUSIONS AND RECOMMENDATIONS -----	55
APPENDIX A -----	57
APPENDIX B -----	66
LIST OF REFERENCES -----	85
INITIAL DISTRIBUTION LIST -----	87

LIST OF FIGURES

1.	Receiver system and instrumentation block diagram -----	13
2.	Receiver calibration block diagram -----	15
3.	Transmitter calibration block diagram -----	16
4.	Aircraft attitude test profile -----	18
5.	Coaxial cable line loss measurement -----	19
6.	Experimental concept with idealized M Profile -----	20
7.	Experimental flight paths -----	21
8.	Flight profile schematic -----	24
9.	Theoretical M Profiles -----	33
10.	Ray traces for surface based duct -----	34
11.	Ray traces for elevated duct -----	35
12.	Mode program predictions for surface based duct -----	38
13.	Loss curve of single mode approximation for surface based duct -----	43
14.	Run 8 M Profiles -----	45
15.	Run 8 Height Gain at 102 nm. with theory using 67 nm. profile -----	46
16.	Run 8 Height Gain at 102 nm. with theory using 10 nm. profile -----	46
17.	Run 8 Height Gain, Vector sum -----	47
18.	Run 8 Loss curve (130 ft.) -----	50
19.	Run 9 Loss curve (150 ft.) -----	51
20.	Run 9 M Profiles -----	52
21.	Run 8 Loss curve (100 ft. below temperature inversion) -----	53

22. Run 9 Loss curve (100 ft. below temperature inversion) ----- 54

ACKNOWLEDGEMENTS

I wish to express my appreciation to Dr. Gordon E. Schacher for his guidance and support in the planning and execution of this research and in helping direct my study effort to provide me with the appropriate academic tools.

My appreciation is also extended to Dr. Jeffrey B. Knorr for the many hours of guidance and special study in propagation theory.

I express special thanks to the following: Mr. Ross M. Seely and Mr. Vic McCullough for their technical assistance in equipment set up and test, Dr. Chris Fairall and Mr. Don E. Spiel for programming assistance, and Mrs. Pat Boyle for assistance in graphics preparation and data reduction.

I would like to thank my family, Phyllis, Clent and Taylor for their sacrifice of our family time to this effort and for enduring and sharing the pressure and the loneliness.

Finally, I thank God for this beautiful universe with whose secrets we vainly dabble.

I. INTRODUCTION

The United States Navy has expended much effort in attempts to measure, model and predict propagation in the atmosphere. This effort is due to the impact the atmosphere has on communication, radar detection and electronic warfare effectiveness. Areas of continued occurrence of nonstandard refractive conditions which produce elevated and surface based ducts have been identified and the operational impact of these conditions has been verified. Recently, operational units have attempted to develop tactics to capitalize on these recurring conditions. The tactics considered have involved positioning aircraft vertically to use duct influences to enhance communication, detection and electronic warfare system performance.

The influences of the ducts on propagation are manifest in the horizontal as well as vertical directions. Propagation in ducts is a multimode phenomenon, as in waveguides, and produces maxima and minima in the horizontal power pattern due to interference of the modes. Waveguide theory has the capability to predict the occurrence of these maxima and minima for a horizontally homogeneous atmospheric duct as well as vertical power variations above and below the duct. Such patterns exist in atmospheric ducting conditions and could be utilized to advantage by ships or

aircraft positioning themselves at appropriate ranges from other transmitter or receiver sites.

The purpose of this experiment was to measure dependence of received power on range within surface based ducts and to compare the measurements to mode theory predictions. The ultimate goal was to determine the feasibility of using the predicted locations of power maxima and minima to position transmitters or receivers. An aircraft with a UHF transmitter covered the range 0 to 150 nm. from a shore based receiver site. Received power was measured continuously and correlated with aircraft range. Three aircraft altitudes were used: 1) 130 ft. altitude, 2) 100 ft. below the temperature inversion, and 3) 100 ft. below the duct top. Three altitudes were used because the strength of the interference pattern and the location of maxima and minima were expected to be a function of altitude.

The Experimental Procedure section of this report describes the equipment, calibration, test methods, and analysis procedures. The Theory section presents the three models studied and their limitations. The Experimental Results section presents two runs representing the best and worst agreement with the theory. Appendix A contains calibration data. Appendix B contains the smoothed data curves from all flights conducted during this experiment.

II. EXPERIMENTAL PROCEDURE

A. EQUIPMENT

1. Aircraft

The aircraft used in this experiment was a Beechcraft Baron equipped with a UHF transmitter and a complete suite of meteorological equipment. All meteorological parameters were measured with a computer controlled digital data acquisition system. Inflight annotations and back up recordings of some parameters were made on an analog strip chart recorder. The equipment description for the aircraft systems, other than the transmitter, is contained in Reference 1.

RF power was supplied by an AN/GRC-171 transmitter coupled to an AN/AT-879A antenna. The antenna was mounted on the center of the underside of the aircraft fuselage, even with the trailing edge of the wing. The AN/GRC-171 is a UHF voice transceiver that was designed for use in military airfield control towers. The AN/AT-879A is a quarter wavelength stub antenna that was designed for use in military aircraft UHF voice communications systems. This antenna provided directional characteristics suitable for the air to ground measurements of this experiment. Detailed descriptions of the AN/GRC-171 and AN/AT-879A are contained in Reference 2 and 3, respectively. Operating conditions for the transmitter system are discussed in the Method

section of this report. All laboratory measurements of system parameters are discussed in the Calibration section.

2. Receiver Site

The receiver site for this experiment was the United States Naval Reserve Center, Pacific Grove, California. The system at the site included the receiver and analog and digital instrumentation for measuring the received power. Receiver site antenna height above ground level was measured to be 8.86 meters. Adding the height above mean sea level of the Pacific Grove Lighthouse of 27 meters yielded the antenna height above mean sea level of 36m. This value was used in all calculations. The receiver system and instrumentation block diagram is presented in Figure 1.

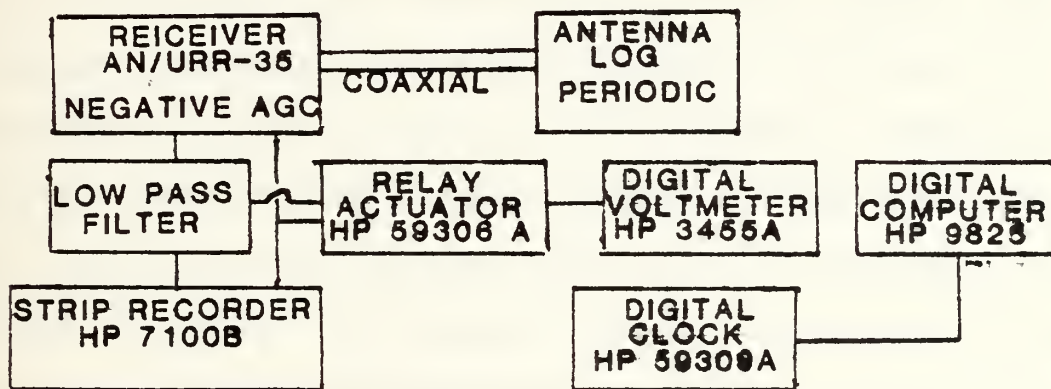


Figure 1.

Receiver System and Instrumentation Block Diagram

The receiver system was an AN/URR-35B equipped with a locally manufactured log periodic antenna. The antenna was mounted on a mast atop the Reserve Center building. The

location of approximately 100 meters from the shoreline, and the antenna elevation of 36 meters above mean sea level provided for minimal terrain interference. The AN/URR-35B is a crystal controlled receiver that was designed for voice communications aboard naval ships. Although the receiver is an older system, with tube components, the replaceable crystal frequency control provided adequate stability for the fixed site installation. A detailed description of the receiver is contained in Reference 4. The receiver's negative AGC voltage output was divided and used for both filtered and and unfiltered inputs to a HP 7100B strip recorder and to a digital data acquisition system. The system consisted of a HP 59306A relay actuator, HP 3455A digital voltmeter, HP 59309A digital clock, and HP 9825 computer. The relay actuator switched the filtered and unfiltered voltages to the digital voltmeter. Recording both filtered and unfiltered voltages allowed separation of the effects of short period and long period changes in the received signal. The computer stored both voltmeter inputs and the time from the digital clock on its internal tape cassette.

B. CALIBRATION

1. Receiver System

Laboratory measurements of the AN/URR-35 receiver negative Automatic Gain Control (AGC) voltage as a function of input power were conducted. The calibration block

diagram is contained in Figure 2. Input power to the receiver was supplied by a HP 608E signal generator at 305.8 megahertz. The signal was coupled to the receiver through

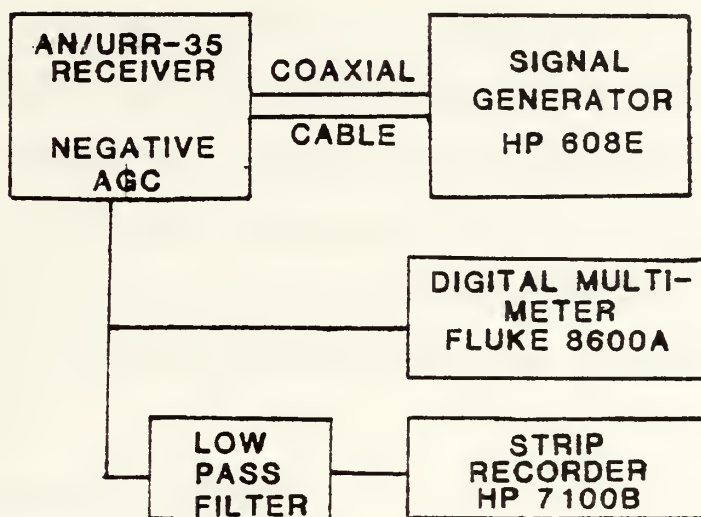


Figure 2

Receiver Calibration Block Diagram

the antenna input. Input power from the signal generator and negative AGC voltage output from the fluke 8600A digital multimeter were hand recorded. Strip recordings of filtered and unfiltered negative AGC voltage were made to calibrate the strip recorder. Filter characteristics are discussed in the Method section. Filter schematic is contained in Appendix A. The plot of AN/URR-35 input power, corrected for line loss, versus negative AGC voltage is contained in Appendix A. Use of the curve for voltage to power conversion is discussed in the Data Analysis section.

Antenna range tests were conducted to determine the relative antenna patterns of the locally manufactured log

periodic antenna. Dipole antenna AN/AT-150 and monopole antenna AN/AS-360 patterns were obtained under similar test conditions to establish an absolute antenna gain estimate. Antenna patterns are contained in Appendix A. The log periodic antenna had gain of 6db above the dipole under the same test conditions. Adding the theoretical gain for a half wavelength dipole antenna of 2.14 dB above isotropic [Ref. 5], the gain for the log periodic antenna was 8.14 dB. Antenna to instrumentation mismatch was neglected for all antenna tests.

2. Transmitter System

Measurements of the AN/GRC-171 transmitter output power and stability were conducted. The calibration block diagram is contained in Figure 3.

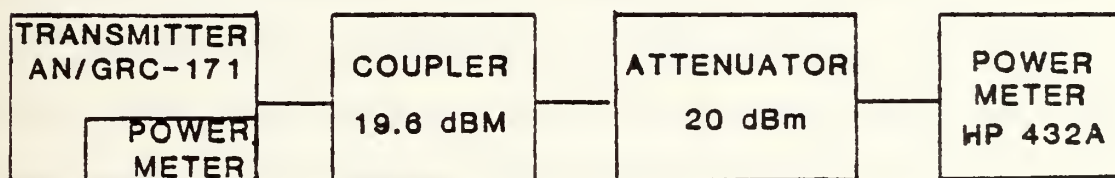


Figure 3.

Transmitter Calibration Block Diagram

The transmitter was coupled to the HP432A power meter through a 19.6 db coupler and 20 db attenuator. The transmitter was operated transmitting a continuous

unmodulated carrier for two hours. For the two hours the transmitter power meter indicated 25 watts and the HP 432A power meter indicated 3.7 dBm, without variation. Adding calibration line losses and converting to power units yielded 21.4 watts output power for a transmitter power meter indication of 25 watts, under laboratory conditions. Variations in electrical power between the laboratory and aircraft were ignored and 21.4 watts was used as transmitter output power for all calculations.

Airborne checks of the transmitter system were conducted to determine if aircraft engine power setting changes would cause detectable changes in received power due to transmitter output variations. The aircraft flew level, constant heading legs centered at 20 nautical miles from the receiver site. Changes in aircraft engine power settings were made and received power recorded on the strip chart. Power settings were used over the full range of aircraft engine power that would be used during the experiment, and there were no detectable variations in received power.

Antenna range tests were conducted to determine the relative antenna patterns of the AN/AT 879A aircraft antenna. Horizontal and vertical antenna patterns are contained in Appendix A. Because there was no capability to establish absolute gain, the manufacturer's specification value of 4 dB above isotropic was used in all calculations. The antenna patterns indicate negligible changes in antenna

gain for small angles off aircraft axis in the vertical and horizontal planes. The negligible changes tentatively indicated that aircraft heading and attitude changes would not influence the received power. Airborne tests were conducted to verify these conclusions.

Two types of tests were performed to determine the effect of the aircraft's attitude on the received power: 1) climbs and descents at constant drift angle to check angle of attack and 2) changes in direction for level flight to check horizontal attitude. To perform test 1) the aircraft flew 1000 ft per minute climbs and 500 ft per minute descents on a constant heading centered at 20 nautical miles from the receiver site. Strip chart recordings of received power were obtained during all maneuvers. Aircraft attitude was adjusted to maintain constant drift angle between aircraft track and aircraft heading. Climbs and descents were performed at zero drift angle with the aircraft heading toward and away from the receiver site. Figure 4 shows the test profile. There were no detectable changes in received

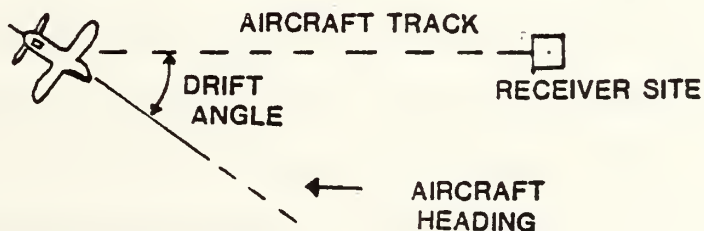


Figure 4.

Aircraft Attitude Test Profile

power as a function of drift angle. There were no detectable changes caused by the angle of attack during climbs or descents. However, large power variations resulted during turning maneuvers and push over and pull up maneuvers at the start and end of descents and climbs. As a result of the conclusions from these tests, all received power data recorded in turning maneuvers or nonsteady portions of climbs and descents were discarded.

3. Coaxial Cables

Laboratory measurements of transmitter and receiver systems coaxial cable line losses were made. The measurement block diagram is shown in Figure 5. A known

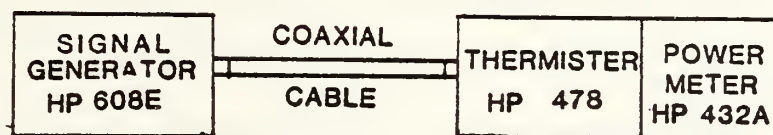


Figure 5.

Coaxial Cable Line Loss Measurement

power of 1 milliwatt (0 dBm) at a frequency of 305.8 megahertz was input in one end of the coaxial and a HP 478 thermistor and an HP 432A power meter were used to record attenuation in decibels below 1 milliwatt (dBm). Appendix A contains the measured values of line loss.

C. METHOD

1. General

Signal measurements, as a function of range and altitude, were made using a transmitting aircraft and a receiver station located on the shore. Figure 6 depicts the experimental concept. The flight procedures were established

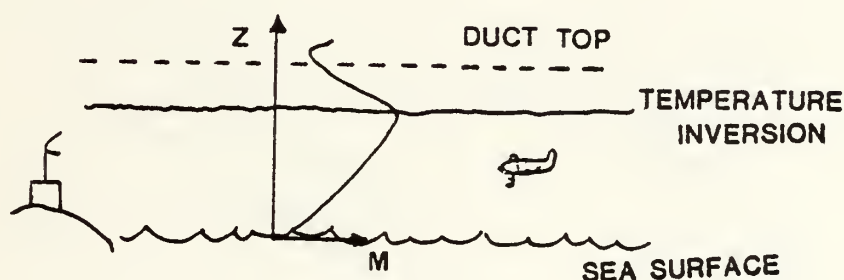


Figure 6.

Experimental concept with idealized M profile

to provide power measurements in the duct below the temperature inversion. Measurements were also taken above the duct for comparison with the in duct measurements. Flight profiles were then developed to determine aircraft influences on power variations. These flight profiles are discussed in the Calibration section.

2. Flight Paths

The experiment was conducted over the Pacific Ocean along the coast of central California in September, 1981. Figure 7 shows the three flight paths that were used during the experiment. Path number one was a constant bearing of

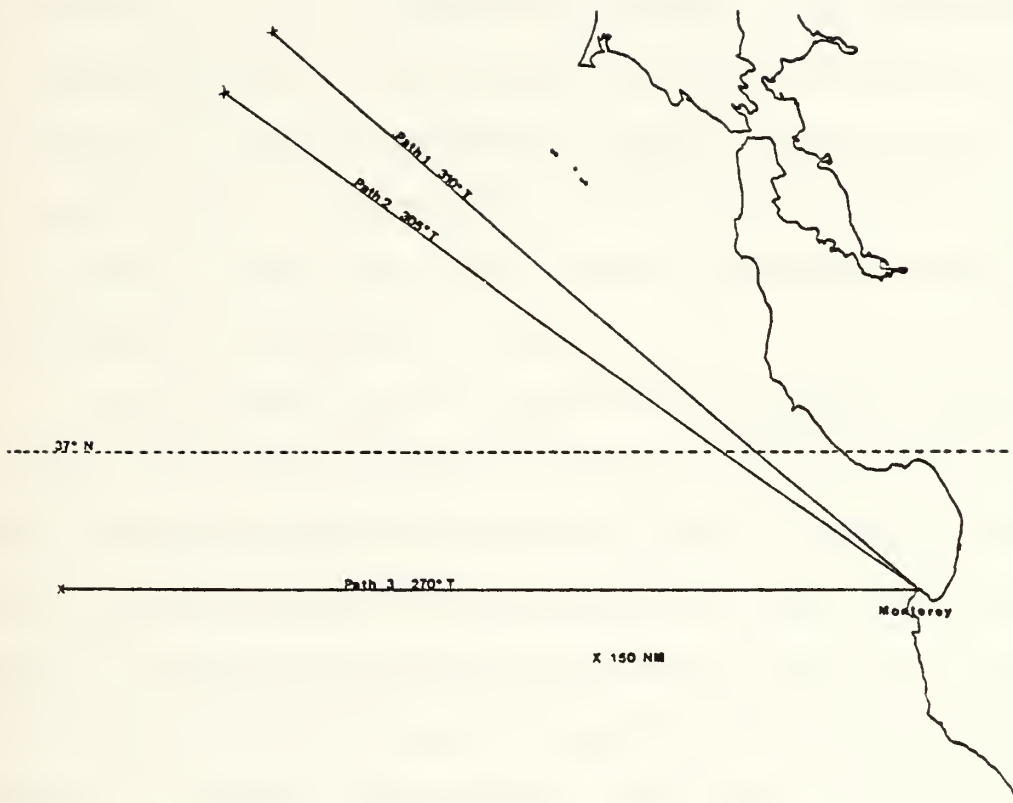


Figure 7.
Experimental Flight Paths

295 degrees magnetic from the receiver site. Path number one was selected for its proximity to land which provided for aircraft safety during warm up flights and during equipment check flights. Path number two was a constant bearing of 285 degrees magnetic from the receiver site. Path number two was used on the majority of data flights because it provided a greater distance from land, reducing land influences on the refractive conditions. These influences are discussed below. Path number three was a constant bearing of 270 degrees magnetic from the receiver site and was perpendicular to the coast. Path number three was flown on the final flight for comparison of refractive conditions with paths more parallel to land.

Path number one was selected in planning because it was theorized that a path parallel to the coast would ensure fairly constant conditions over the path. Surface based ducts could be expected near land due to the circulation patterns produced by prevailing westerly winds. The vertical convection overland during the daytime heating cycle was expected to produce circulation aloft from land to sea and descending air over the water near the coastline. This descending air over the water, referred to as local subsidence, was expected to produce lower inversion heights near land. However, for the conditions of these experiments, this effect occurred only at distances less than approximately ten nautical miles from land. Path one

did not produce the desired horizontal homogeneity. For two reasons path one was abandoned in favor of path two. First, aircraft navigation required a path farther from shore at long ranges from the receiver site. At the long range end of path one the aircraft was near a line drawn between the two strongest loran stations. On this line, called a baseline, the loran fixes were intermittent and aircraft range data were lost. Second, proximity to land and low aircraft altitudes used in the experiment introduced a safety problem on path one in conditions of low clouds. For these reasons, path two was preferred.

3. Flight Profiles

Figure 8 depicts a schematic of the flight profile used for the experiment. The aircraft initially performed a turning climb (spiral sounding) at approximately 10 nm. (18.5km) from the receiver site to obtain meteorological data. The spiral soundings started at 10 ft. (3m) from the surface and continued to at least 3000 ft. (909m) altitude. The aircraft then proceeded to over the receiver site and commenced the outbound flight on a constant bearing path. The initial altitude was 100ft. (30m) below the temperature inversion, as determined by the 10 nm spiral sounding. At range intervals of approximately 30 nm. (56km) the aircraft performed climbs at 500 ft. (151.5m) per minute rate to an altitude where the temperature gradient was again negative. The aircraft flew approximately one minute level at altitude

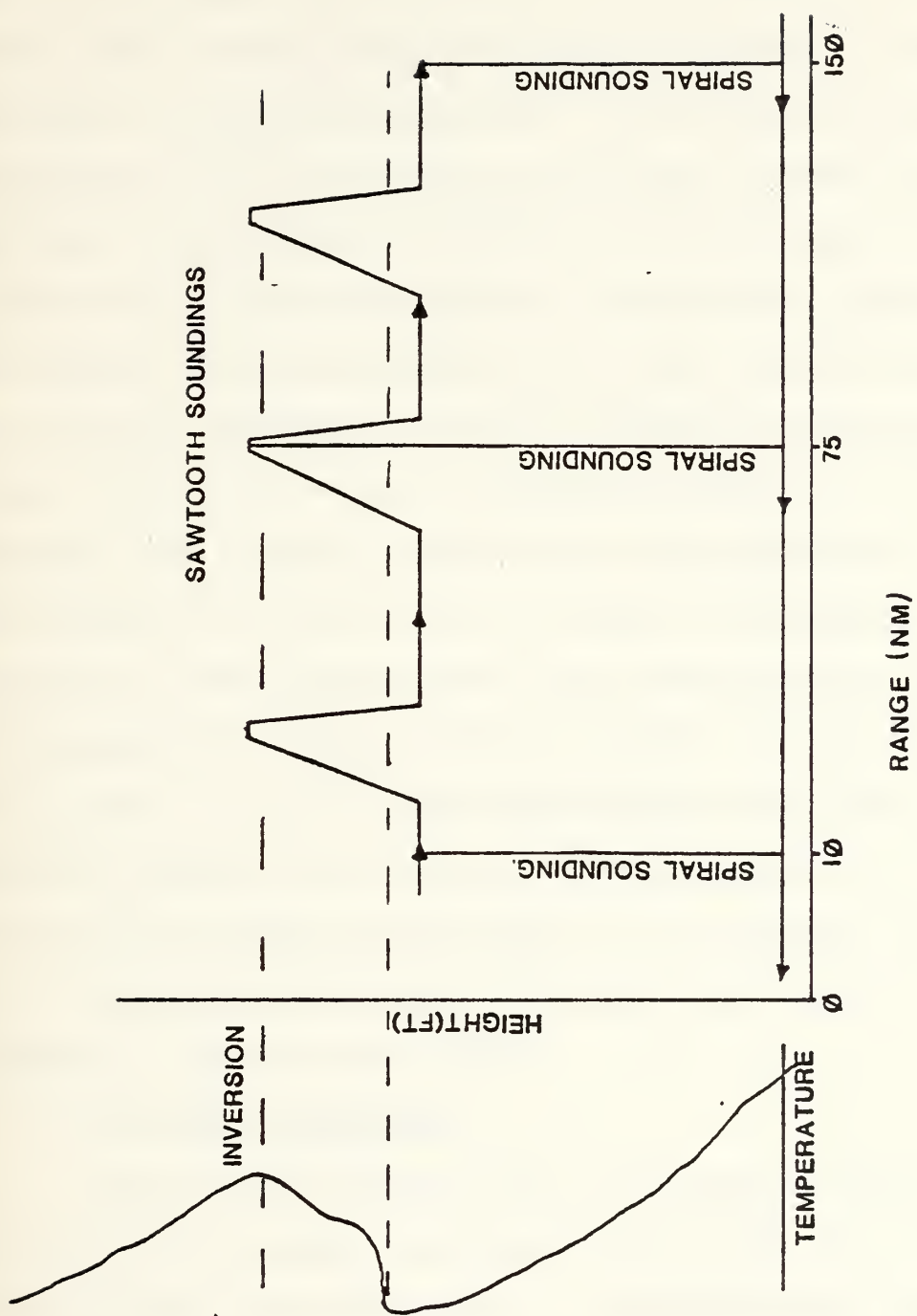


Figure 8.
Flight Profile Schematic

and then performed a descent at 1000 ft. (303 m) per minute rate to a new altitude. This new altitude was 100 ft. (30m) below the temperature inversion as determined by the last climb. The entire climb and descent sequence is referred to hereafter as sawtooth soundings. The sawtooth procedure was interrupted at 75 nm (139km) to perform a second spiral sounding. The sawtooth procedure continued again from 75 nm (139km) to 150 nm (278km) where a third spiral sounding was performed. After completion of the third spiral sounding the aircraft descended to 130 ft. (40m) and proceeded back toward the receiver site at constant altitude on reciprocal bearing. The aircraft periodically descended to 10 ft (.3m) and returned to 130 ft (40m) to reset the pressure altimeter. After passing over the receiver site the run was terminated with a fourth spiral sounding at approximately 10 nm (18.5km). On one flight the procedure was modified so that the maximum level flight time was at 6000 ft (1829m). This high altitude data was taken to be compared with the data in and below the duct. Appendix A contains a table of flights and flight conditions.

4. Aircraft Procedures

The GRC-171 transmitted a continuous unmodulated carrier at 305.8 MHz. Indicated output power was 25 watts on the transmitter power meter. The power meter was monitored periodically and during conditions of exceptional variations of received power. No deviations from 25 watts

indicated output power were discerned during any check. The aircraft digital system recorded atmospheric pressure, temperature and dew point temperature. Also recorded digitally were time and loran position in latitude and longitude. Digital data were taken continuously during aircraft flights at sample intervals of approximately 2.5 seconds or 4.5 seconds depending on the flight. An analog strip recorder recorded atmospheric pressure, temperature and dew point and aircraft altitude. Coordination with the receiver site was conducted on Very High Frequency (VHF) voice radio and hand annotations were made of aircraft range and bearing from the receiver site at approximately 10 nm (18.5km) intervals as back up information. Times of climbs, descents, turns, radio transmissions, aircraft heading, aircraft ground speeds, and other events such as clear air turbulence were also hand recorded on both the aircraft strip chart and the receiver site strip chart.

5. Receiver Site Procedures

The receiver site digital data acquisition system recorded receiver negative automatic gain control (AGC) voltage from the AN/URR-35. Recordings were made of both unfiltered and filtered AGC voltage. Filtered voltages were from a .1 MHz low pass filter. For this experiment, primary interest was in low frequency variations in received power. These variations were produced by the aircraft traversing the power patterns in the duct. Higher frequency variations

in received signal were produced by aircraft antenna pattern motion and phase changes in the reflected path caused by ocean surface wave action. The high frequency variations were eliminated in the filtered voltages. Filtered voltage was used in all data analysis discussed below.

Time was also recorded digitally. Digital receiver AGC voltage measurements were taken continuously during the aircraft flights at a sample interval of approximately .1 seconds. One hundred samples were averaged to provide a 10 second sample interval for stored AGC voltage data. An analog strip recording of filtered and unfiltered receiver AGC voltage was made and hand annotated in the same manner as the aircraft strip chart recording described above.

D. DATA ANALYSIS

1. General

Analysis of the aircraft meteorological data and receiver site AGC voltage data produced three types of plots: M versus height (M profiles), received power versus range (loss curves), and receive power versus height (height gain curves). This section describes data analysis processes, including the conversions, editing procedures, and estimates used to attain the final graphs.

2. Loss curves

Annotations of times and aircraft ranges on both aircraft and receiver strip charts were used manually to establish a table of times versus ranges for each flight.

Intermediate ranges were estimated using the average aircraft velocity between the recorded points. The time periods were edited to eliminate aircraft climbs, descents or turns. The remaining times and ranges were used in a digital program to perform a time search of the receiver site voltage data producing a matrix of range versus negative AGC voltage for each flight. The negative AGC voltage was then converted to relative received power in decibels below a milliwatt (dbm) using the AN/URR-35 calibration curves.

The computer power conversion equations were established by regression analysis of the calibration points. The calibration curves and the power conversion coefficients are contained in Appendix A.

The points for each loss curve were grouped and plotted according to aircraft altitude. Low altitude (40m) data were taken at constant pressure altitude over the entire range and are grouped in one plot. However, high altitude data were taken in level flight at various pressure altitudes, either 100 ft (30.3m) below the temperature inversion or above the duct top. The data for 100 ft (30.3m) below the temperature inversion are grouped in one plot for each flight and the data above the duct top were grouped in one plot for each flight. Variations in aircraft height due to variations of the temperature inversion height were not noted on the plots.

For each power plot a received power threshold was established from the negative AGC voltage with the aircraft transmitter power off. The zero input AGC voltage was converted to relative received power in dbm using the calibration curves. This receiver threshold was used to establish the point below which receiver signal was considered not measurable. Points below the receiver threshold were eliminated. Missing data due to climbs or descents for range intervals of greater than 10 nm (18.5km) were indicated as gaps in the loss curves.

3. M Profiles

Plots of modified refractivity units (M units) versus height above the surface were made from measurements of atmospheric temperature, pressure, and dew point temperature taken by the aircraft. Aircraft measurements were made during climbs and descents. Occasionally, gust conditions caused the aircraft climbs or descents to be nonmonotonic. The points were edited to provide a monotonic increase or decrease in aircraft height with time. Aircraft altitude for each climb or descent was digitally recorded in pressure altitude and was referenced to the 10 ft (3.03m) pressure taken by the aircraft. On soundings for which the aircraft did not descend to 10 ft (3.03m) the 10 ft (3.03m) pressure measurement closest in range to the sounding was used as a reference value. Synoptic variations in surface pressure from sounding to reference point were ignored.

4. Height Gain Curves

Received power versus height (height gain curves) were taken from sawtooth climb and descent data. Spiral soundings were not used for height gain because aircraft turns influenced the measurements. The aircraft digital acquisition system recorded pressure altitude at 2.5 or 4.5 measurements per second as discussed above. Listings of aircraft pressure altitudes and times were used to manually select receiver AGC voltage points from the analog strip chart data. Tables of receiver AGC voltage versus aircraft pressure altitude were edited to provide monotonic height information. The tables were then manually entered into the digital computer for conversion to received power, for storage and for plotting. Height gain curves were identified with the average range for the climb or descent period. Duct top and bottom points from the sawtooth M profiles and the free space received power computed from calibration data were included on the height gain curves as reference information.

III. THEORY

A. GENERAL

Three methods of analysis of RF propagation in the atmosphere were considered in this study: 1) ray theory, 2) waveguide mode theory and 3) a single mode approximation to the mode theory. This section provides general discussion, presents characteristic output curves and discusses the advantages and limitations of each method. A presentation of the general theory of atmospheric effects on propagation with basic definitions is contained in references 6 and 7.

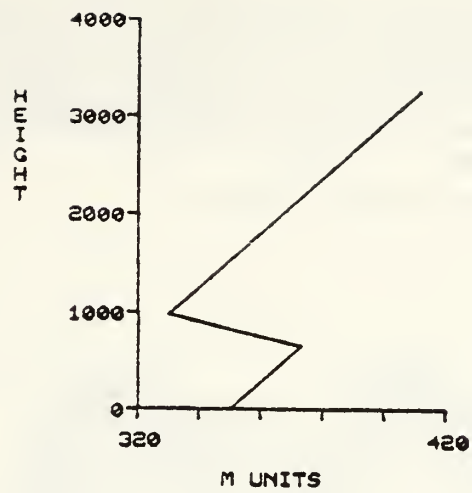
B. RAY THEORY

Ray theory considers the propagation paths to be rays which are defined as "normals to the surfaces of constant phase of the wavefronts." [Ref 8]. Using Snell's Law, ray theory predicts the effect of refraction on the direction of propagation without regard to the wavelength or the phase of the waves.

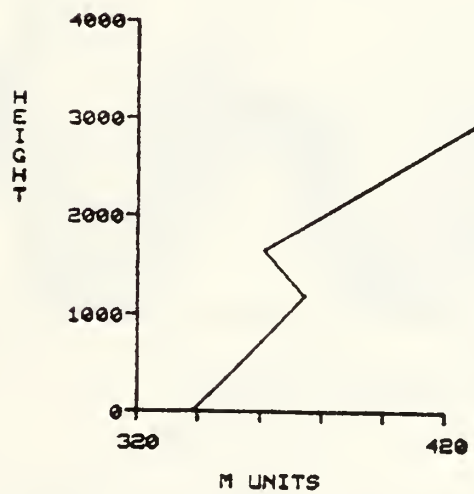
The ray tracing program used in this experiment was developed by the Naval Ocean Systems Center, San Diego, California, and is presented in detail in Reference 9. Ray path predictions from this program were used to identify the refractive conditions under which the power variations with range in the duct were expected to be greatest. These conditions were desired for the experiment to facilitate the

measurement of the location in range of the maximum and minimum power points. Figure 9a is an M profile which yields a surface based duct, used in planning the experiment. Figure 10 (a) to (c) are the ray traces using M profile of Figure 9 for three transmitter altitudes: 1) 130 ft. from the surface, 2) 100 ft. below the temperature inversion and 3) 100 ft. below the duct top. All three ray traces predict maxima and minima in the received power as a function of range. Figure 10 (c) indicates that the transmitter in the duct, 100 ft. below the duct top, provides the most pronounced concentration of rays at the surface maxima. This implies that receive power maxima and minima would be strongest for the aircraft at this altitude relative to the duct.

Figure 9 (b) is a theoretical trilinear M profile yielding an elevated duct. Figure 11 (a) to (c) is the ray trace using the same three transmitter altitudes relative to the duct. The ray traces of Figure 11 indicate that the occurrence of maxima and minima in the received power at the surface would not be expected for elevated ducts. These predictions indicate a clear distinction between received power patterns at the surface for surface based and elevated ducts. Two factors limit the validity of this simple prediction. First, the lack of phase information makes conclusions concerning power distribution questionable. Second, there is leakage of power out of a duct where ray



(a)



(b)

Figure 9.

Theoretical M Profiles (a) Surface Based (b) Elevated

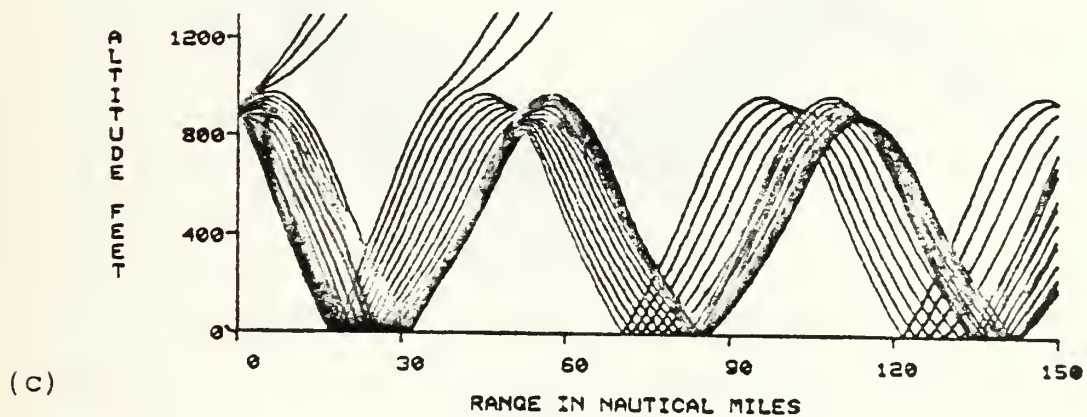
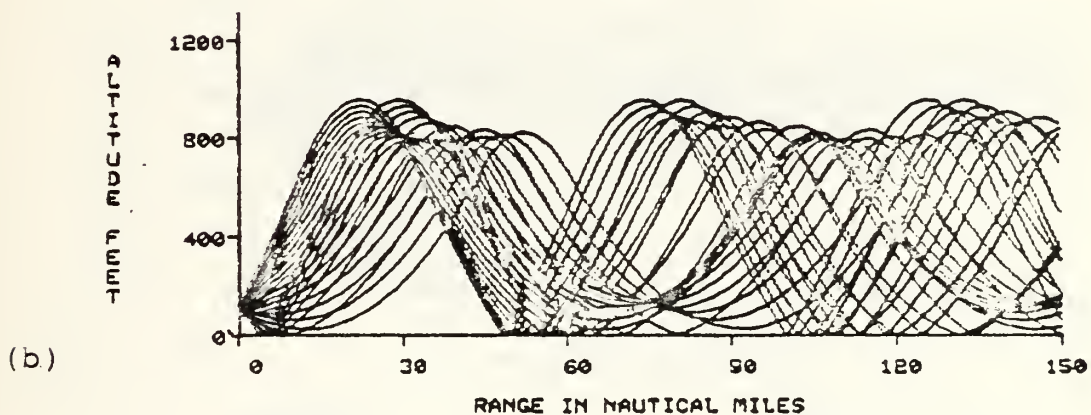
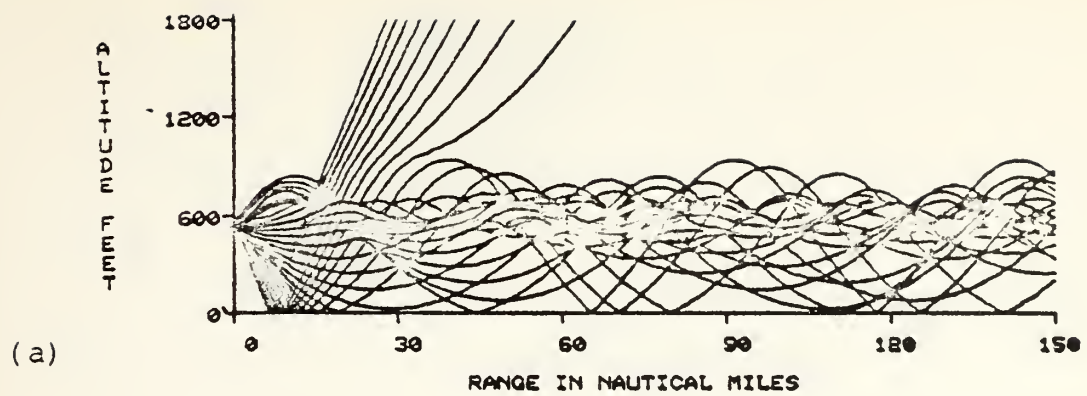


Figure 10.

Ray traces for surface based duct (a) Transmitter at 130 ft. Altitude (b) 100 ft. below temperature inversion (c) 100 ft. below duct top.

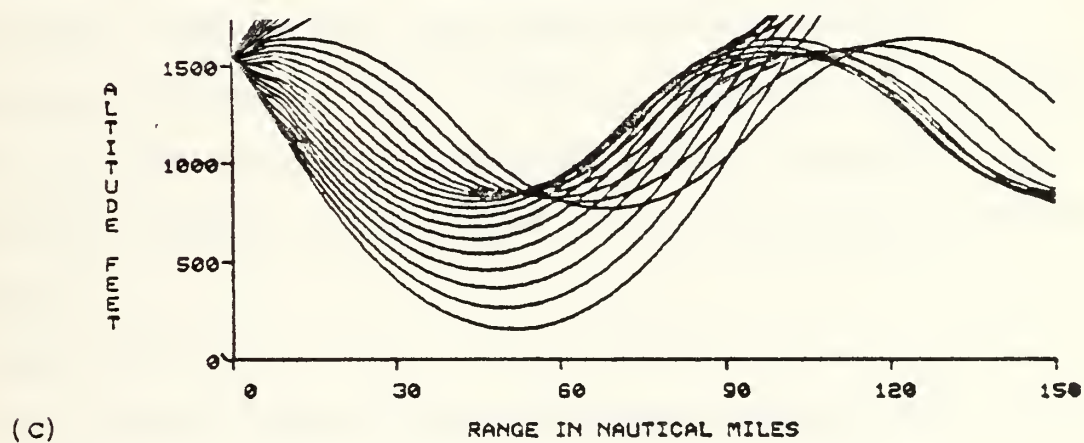
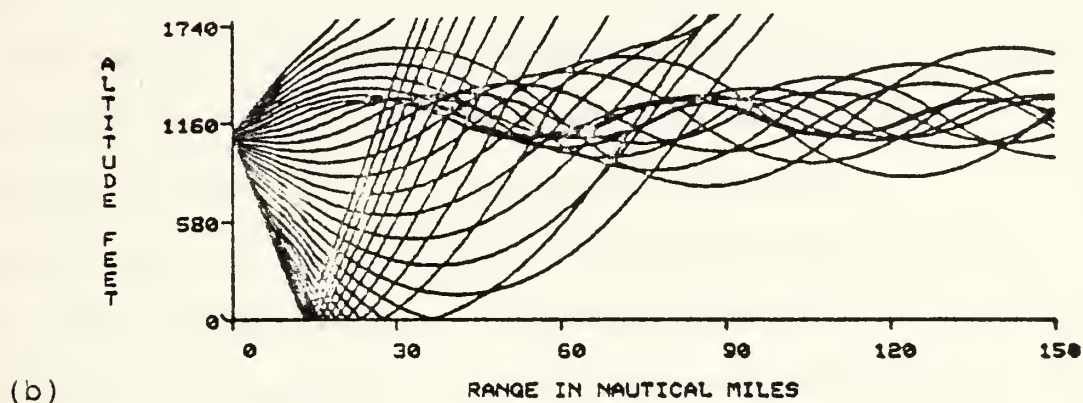
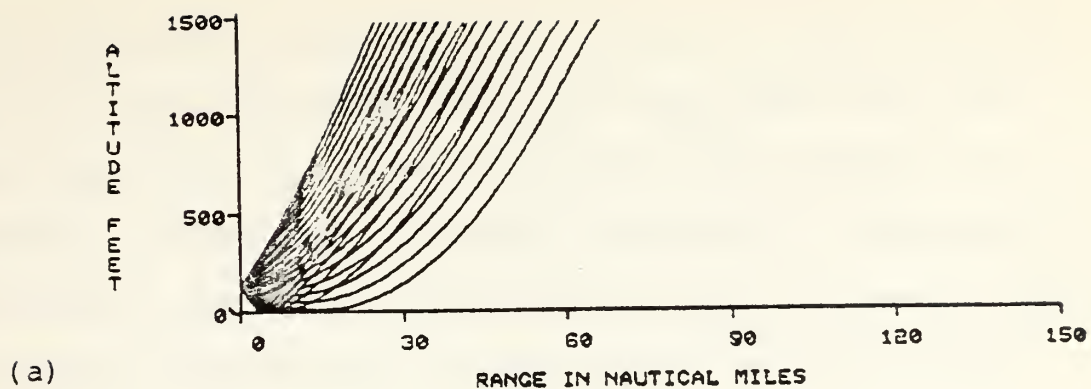


Figure 11.

Ray traces for elevated duct (a) Transmitter at 130 ft.

(b) 100 ft. below temperature inversion

(c) 100 ft. below duct top.

theory indicates total trapping. These two factors would tend to reduce the power maxima and feed power into the minima resulting in a less pronounced power pattern as a function of range for the surface based duct. The power of high order, leaky modes outside an elevated duct would tend to produce a maximum and minimum pattern at the surface where none was predicted by ray theory.

Ray theory is effective in providing a simple graphical view of the nature of refractive effects but does not provide a quantitative representation of energy distribution. Ray theory breaks down for prediction of energy distribution because the phase difference of various refracted paths arriving at a point are not considered. The ray program used in this experiment did not consider horizontal changes in the M profile. Reference 10 considers horizontal changes in the M profile for ray tracing. These horizontal changes are discussed in the Experimental Results section.

C. MODE THEORY

Mode theory accounts for wavelength, phase, and penetration of the boundaries and predicts the energy distribution. The atmosphere is treated as a waveguide with losses [Ref 11]. A multimode solution to the wave equation is provided, incorporating nonstandard refractive conditions. The waveguide mode program used in this experiment was developed by the Naval Ocean Systems Center,

San Diego, California, and is presented in detail in Reference 12. Two experimental verifications of the waveguide mode program are contained in References 13 (Pappert, et. al.) and 14 (Skillman and Woods). Comparison of these verifications to this experiment is contained in the Experimental Results section.

waveguide mode programs generally calculate power in two ways. The coherent or vector sum takes the vector sum of the power density from the magnitude of the resultant field. The vector sum accounts for a definite phase relationship among modes at a point [Ref 15]. The incoherent or power sum takes the sum of the power of the modes at a point. This sum is the expected value of the power for the modes assuming uniformly distributed phase. The vector sum exhibits more variation in the height gain curve due to phase interaction of the modes. The power sum yields better agreement for average power levels at long range due to the random phase relationship of the modes at long range [Ref 16]. The random phase possibly results from duct non-uniformity. The waveguide program predictions were compared to the measurements of this experiment and are presented in the Experimental Results section.

Figure 12 contains waveguide mode predictions from the mode program for the theoretical surface based M profile of Figure 9 (a). The waveguide mode program outputs propagation loss from the transmitting antenna to the

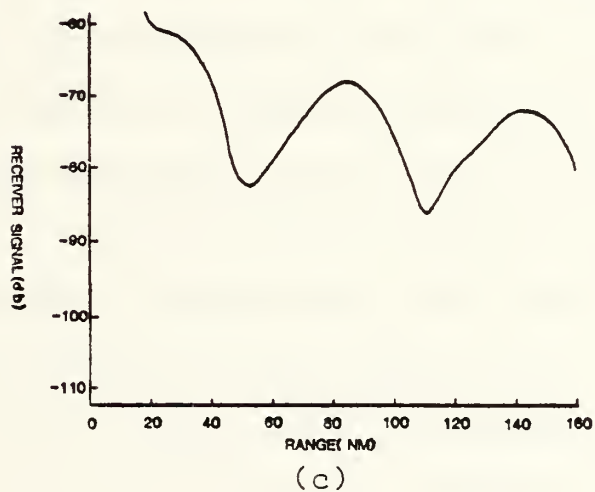
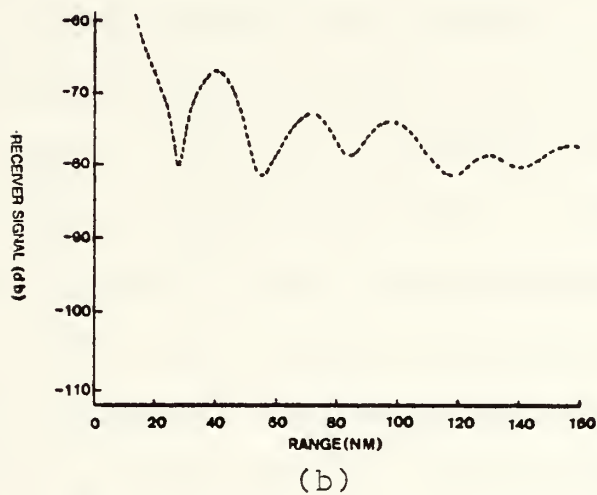
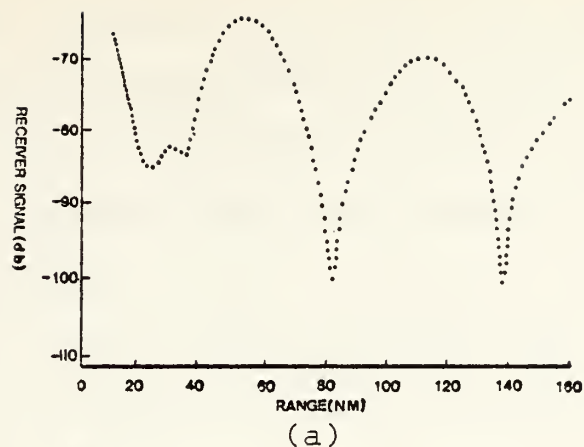


Figure 12.

Mode program predictions for surface based duct
 (a) Transmitter at 130 ft. altitude (b) 100 ft. below
 temperature inversion (c) 100 ft. below duct top.

receive antenna. Figure 12 has been referenced to the equipment used in this experiment for direct comparison with experimental data. The propagation loss predictions of Figure 12 were computed for three aircraft altitudes: 1) 130 ft. from the surface, 2) 150 ft. below the temperature inversion and 3) 150 ft. below the duct top. As in the ray traces for this profile, all three plots predict maxima and minima in the received power as a function of range. The aircraft altitude effects the depth of the maxima and their spacing with range. For 130 ft. aircraft altitude, Figure 12 predicts minima at approximately 20, 80, and 140 nm. The power excursions, peak to null, are predicted to be approximately 40 db. For aircraft altitude 150 ft. below the temperature inversion, the period has decreased and the power excursions are less than for the previous altitude. Minima occur at approximately 25, 55, 85, 115 and 140 nm. Maximum power excursion of approximately 15 db at near range decreases to approximately 5 db at 140 nm. For aircraft altitude 150 ft. below the top of the duct, the spacing and the power excursions increase over that for the previous altitude. Minima occur at approximately 50, 110 and 160 nm. The power at 150 ft. below the duct top is a maximum when power at 130 ft. is at a minimum. Figure 12 implies that aircraft height might be chosen to maximize or minimize the received signal for a given surface based duct condition.

The mode program used in this experiment is limited by

three factors. First, the program does not account for the presence of the evaporation duct [Ref 17], a low level ground based duct usually present over the ocean to a height of approximately 10 meters. This duct traps energy near the surface when either or both the transmitter and receiver antenna falls in the duct and would tend to enhance power within a higher surface based duct. Second, this program uses an average M profile and assumes the refractive conditions are homogeneous with range. The horizontal change in the boundaries of the duct in a waveguide multimode problem will cause conversion of energy between modes [Ref 18]. If the conversion is from highly attenuated modes to modes with lower attenuation, the actual losses in the waveguide would be less than predicted by the mode program. Third, accurate solution of the multimode problem requires finding the roots to the wave equation with the mode condition applied. Failure to identify all the significant roots of the equation may limit the accuracy of the solution of received power at a point. Initial parameters are required, such as the height for unity refractive index and the reference height for the reflection coefficient in the duct [Ref 19]. In some cases changing these parameters can provide for more modes in the solution for significant roots [Ref 20]. These additional modes could provide for more power trapped in the duct than predicted if the roots were missed. The problem of missing

modes can only be corrected if there is a known experimental standard to which the results of the program can be compared. As discussed above, the program assumes an average homogeneous profile. Therefore, no such standard can be applied for the case of extreme nonuniformity in M profile. The implications of these three restrictions are discussed in the Experimental Results section.

D. SINGLE MODE APPROXIMATION

The single mode approximation to the waveguide mode theory provides a simple estimate of a solution to the wave equation for surface based duct conditions. The single mode approximation is included in the Integrated Refractive Effects Prediction System (IREPS). IREPS was developed by the Naval Ocean Systems Center, San Diego, California and is discussed in reference 21.

Path loss for this model is computed for three regions:

1) Interference 2) Intermediate 3) Diffraction. The interference region extends to the effective horizon (geometric horizon modified for refractive conditions). In the interference region, the received power is computed using a program which calculates phase difference by accounting for path length, compensation for curved earth and change in reflection coefficient due to conductivity of the ocean. The intermediate region is beyond but near the effective horizon and is that region in which the diffraction solutions cannot use a single mode estimate. In

the intermediate region a straight line interpolation of power levels between the interference and the diffraction regions is used. The diffraction region is well beyond the horizon. In this region the program computes loss for ducted signals using empirically established height gain functions for the transmitter and receiver and an attenuation factor for the single primary mode.

Figures 13 (a) to (c) are the predicted loss curves from the single mode program using the theoretical trilinear M profile of Figure 9 (a). These curves are predictions for received power for the three aircraft altitudes used in the previous section. There are predictions of maxima and minima in the interference region for Figure 13 (a), but none are predicted in the diffraction region for any curve. This lack of diffraction region power pattern, other than a monotonic decrease, is caused by the assumption that the height gain curves for the diffraction region are not a function of range.

The limitations of the single mode program to surface based duct conditions and the assumption that the height gain curves are independent of range are severe restrictions. The single mode program could not be used in this study to predict the envelope of the loss curve in the diffraction region because it ignores the range versus power variations that this study sought to investigate.

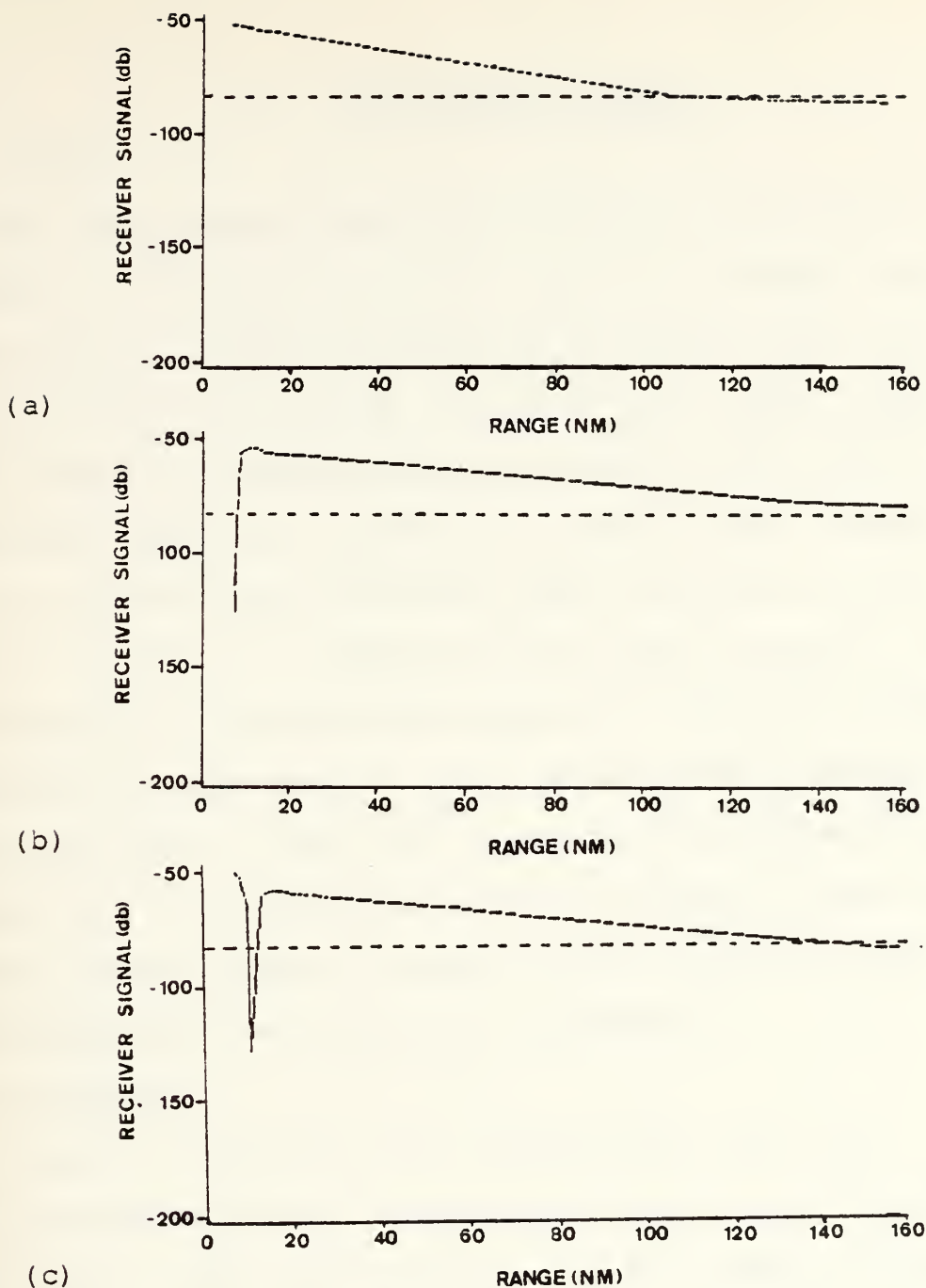


Figure 13. Loss curves. Single mode approximation. Surface based duct. Dashed line is free space power at 160 nm. (a) 130 ft. altitude (b) 100 ft. below temperature inversion (c) 100 ft. below duct top.

IV. EXPERIMENTAL RESULTS

A. GENERAL

The experimental data were reduced to five types of curves: 1) M profiles for each flight on a height versus range graph, 2) height gain curves for each flight on a height versus range graph, 3) for one run (run 3) the height gain curves are plotted with the waveguide mode theory predicted height gain curves, 4) received power versus range for the aircraft below the duct near the earth's surface (130 to 200 ft.), 5) received power versus range for the aircraft 100 ft. below the temperature inversion. Appendix B contains the experimental data for all flights conducted in this experiment. Runs 8 and 9 typify the extremes in the results and the discussion below is limited to these runs. A table of duct tops and bottoms for all soundings taken in this experiment are contained in Appendix A.

B. M PROFILES

Figure 14 contains the M profiles for run 8 and illustrates the general refractive conditions during the experiment. The duct is elevated at all ranges. The duct top varies approximately 240 meters, maximum to minimum, and rises approximately 200 meters from near the receiver to long range. The surface based conditions desired in the planning of the experiment were never realized and the conditions of nonuniformity in M with range were observed

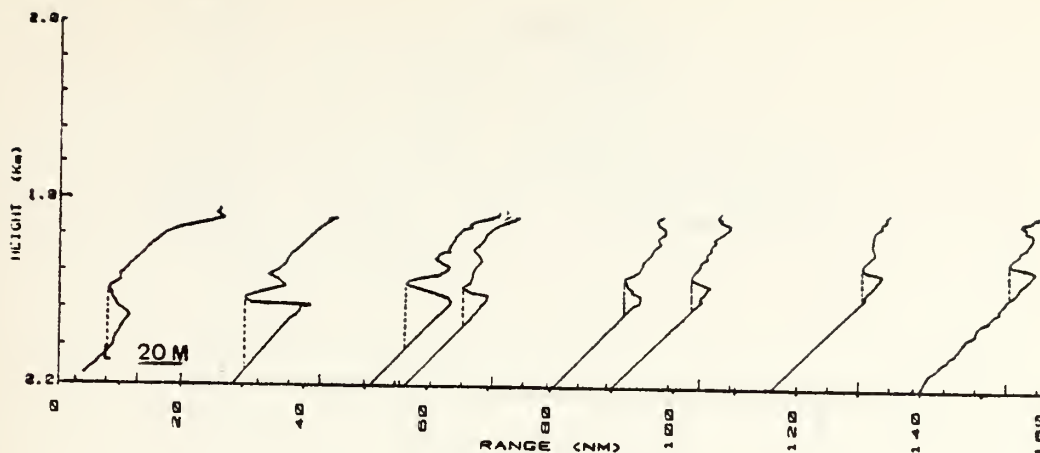


Figure 14.

Run 8 M Profiles

for all runs. The influence of local subsidence mentioned above reduced elevated duct heights near land and caused a sloping of the duct height up and away from the receiver site.

C. HEIGHT GAIN CURVES

Figure 15 is a height gain curve from run 8 taken at 102 nm. average range. Included in Figure 15 is the waveguide mode program power sum output using the 67 nm. M profile of Figure 14 as the average profile. The predicted power does not follow either the average level below free space or the envelope features of the measured curve. Figure 16 is the same height gain compared to waveguide mode program power sum output for the 10 nm. M profile of Figure 14. agreement but does not produce the envelope features of the measured curve. Figure 17 (a) and (b) are comparisons of

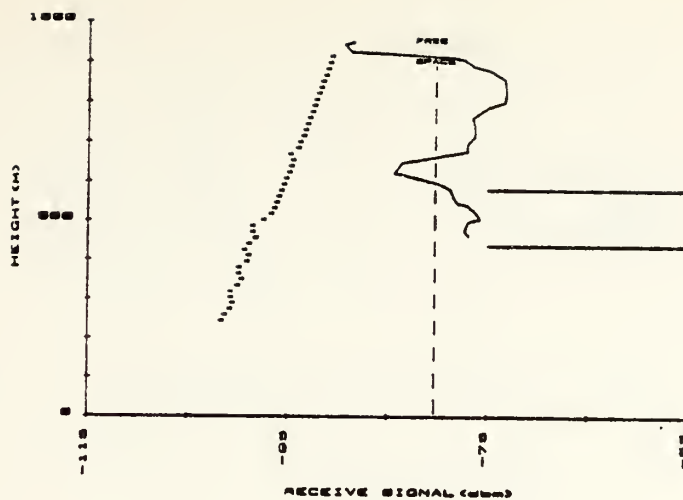


Figure 15.

Run 8 Height Gain for 102 nm. (solid line)
and Theory using 67 nm. M Profile (bars)

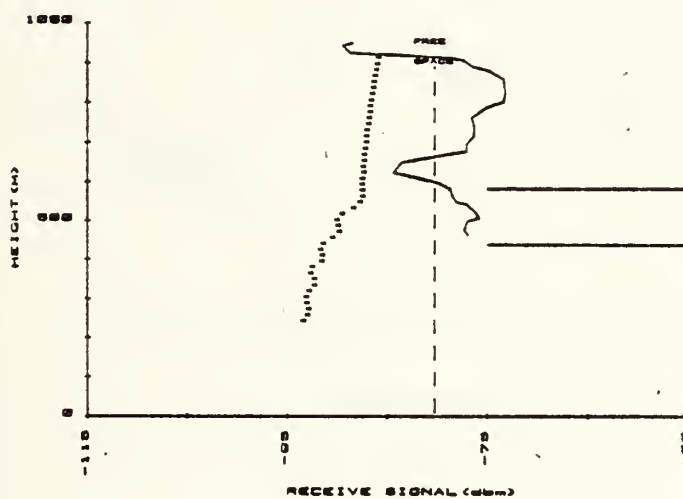
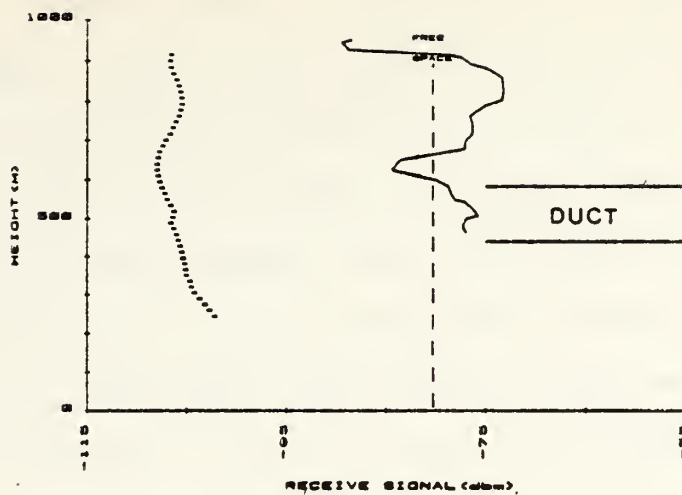
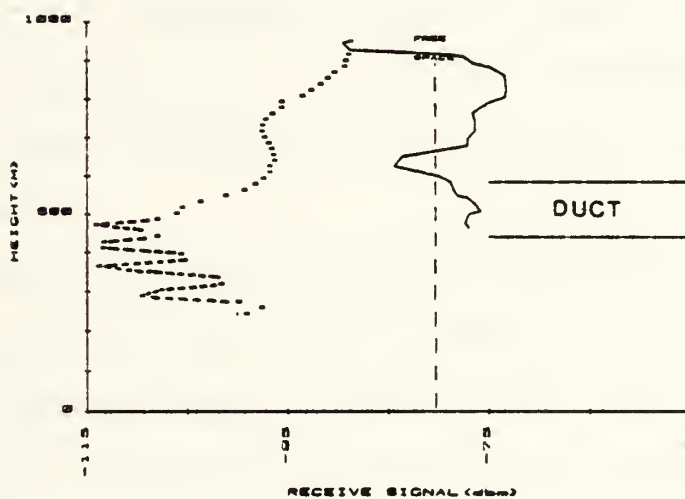


Figure 16.

Run 8 Height Gain for 102 nm. (solid line)
and Theory using 10 nm. M Profile (bars)



(a)



(b)

Figure 17.

Run 8 Height Gain at 102 nm. (solid line) and Vector sum theory (bars) for (a) 67 nm. profile (b) 10 nm. profile

the 102 nm. measured height gain with the waveguide mode program vector sum for the 67 nm. and the 10 nm. M profiles. The 67 nm. profile provides better agreement with measured envelope features in and above the duct. Both vector sum cases predict lower average power level for the power sum is in closer agreement with the measured values. Similar conclusion for the vector sum average power was reached by Skillman and Woods, but their vector sum envelope agreement was better. The figures presented here are characteristic of the lack of agreement between theory and measurement in this experiment. Measured height gains show power levels within 10db of free space with envelope features varying approximately 5db above and below free space. Predicted height gains are as much as 30 db lower than measured and predict envelope features varying less than a few db from the mean power.

Selection of the 10nm. M profile provided better average power agreement for the power sum than the 67 nm. M profile. The better agreement may be due to the 10 nm. M profile which yielded a wider duct and provided for more lower attenuation modes. These modes would yield a higher average power. The vector sum provided some improvement in agreement for the 67 nm. M profile but poor agreement for the 10 nm M profile.

The agreement between waveguide mode theory and measured height gain curves in this experiment is not as

good as previous experimental verification made by Pappert and Skillman. In the experiment of Pappert, the refractivity conditions produced wide surface based ducts, that were nearly uniform with range. The surface based conditions would yield solutions with fewer significant leaky modes. The fewer leaky modes would simplify the solution and improve agreement. In the experiment of Skillman, the refractivity conditions produced very high elevated ducts nonuniform in range. However, power measurements of Skillman were made at much greater ranges into the diffraction region than this experiment. Solutions improve at greater distances from the horizon [Ref 22], which may account for Skillman's better agreement between theory and measurement.

The limitation of the waveguide mode program to an average M profile could be the most significant factor causing the discrepancy between theory and measurement in this experiment. The tilt of an elevated layer enhances trapping [Ref 22] and maintains propagation power above that for a horizontal duct. The effect of nonuniformity in the M profile with range and proximity to the horizon of this experiment could explain the measurement of average powers higher than theoretical.

D. LOSS CURVES

1. Aircraft Below The Duct

Figure 18 is the loss curve for run 3 for the aircraft altitude of 130 ft. The curve shows interference

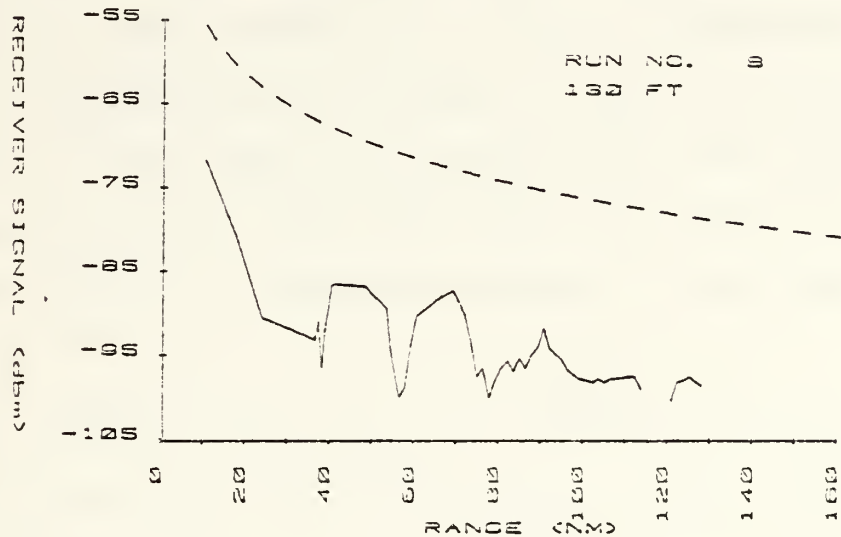


Figure 18.

Run 3 Loss Curve. Aircraft altitude 130 ft.

dashed line is calculated free space power.

maxima and minima from 30 nm. to 100 nm. range. There are minima of 15 db depth at approximately 35, 55 and 75 nm. The interference pattern is not present at ranges greater than 80 nm. The average power for this run is approximately 20 db below free space. This run produced the best defined interference structure of the experiment. The envelope of the curve of Figure 18 compares favorably with the theoretical patterns predicted by Figure 12 (a). The elevated ducts of run 3 could be expected to contain high order leaky modes that would produce interference power

patterns below the duct similar to those expected in the duct. Figure 18 patterns are of shorter period and have a smaller peak to null power difference than those of Figure 12 (a). Differences in the character of the curves are to be expected since Figure 12 (a) is for a theoretical M profile yielding a surface based duct but the measurements of Figure 18 were taken in elevated duct conditions.

Figure 19 is the loss curve for run 9 for an aircraft altitude of 150 ft. The power envelope of this curve does

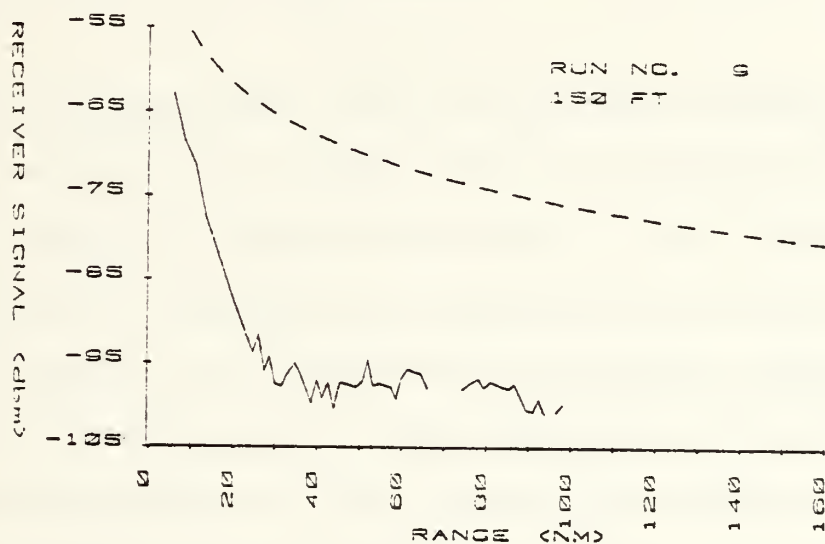


Figure 19.

Run 9 Loss Curve. Aircraft altitude 150 ft.

Dashed line is calculated free space power.

not exhibit significant features or a recognizable period. Figure 20 contains the M profiles for run 9. The refractivity conditions vary in two respects from those of run 8 (shown in Figure 14). First, the near range duct width is greater in run 8. The wider duct allows for fewer

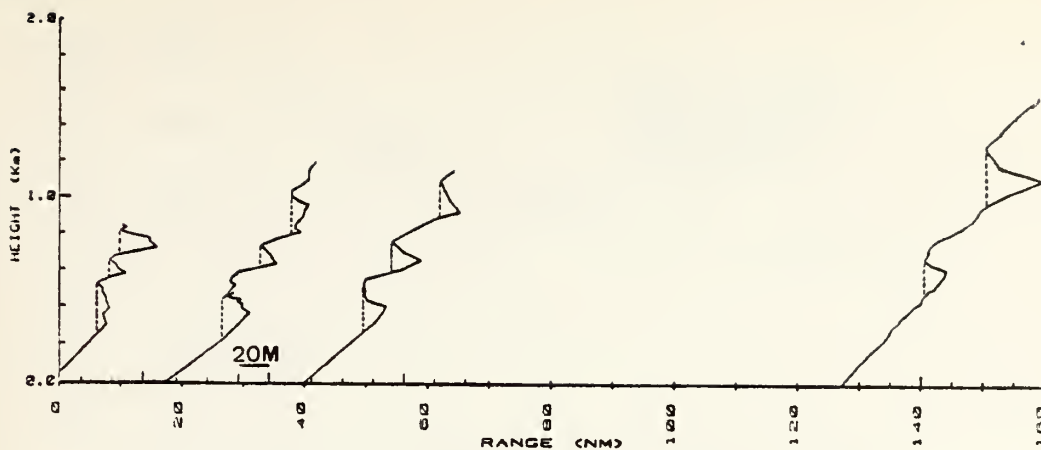


Figure 20.

Run 9 M Profiles

high order leaky modes, less interference between modes below the duct, and a recognizable interference pattern. The larger number of higher order modes in run 9 accounts for the absence of recognizable interference patterns below the duct. Second, run 9 refractivity structure contains multiple elevated ducts. Modes coupled to the higher ducts would have leakage out the top and interference patterns of their own below the multiple duct system. The leakage and interference patterns would tend to destroy the envelope of the lower ducts through interference. The narrower duct system and the multiple duct system would account for the lack of recognizable period to run 9 data.

2. Aircraft in the Duct

Figure 21 is the loss curve for run 3 for aircraft altitude 100 ft. below the temperature inversion. The curve shows average power levels within 5db of free space. These

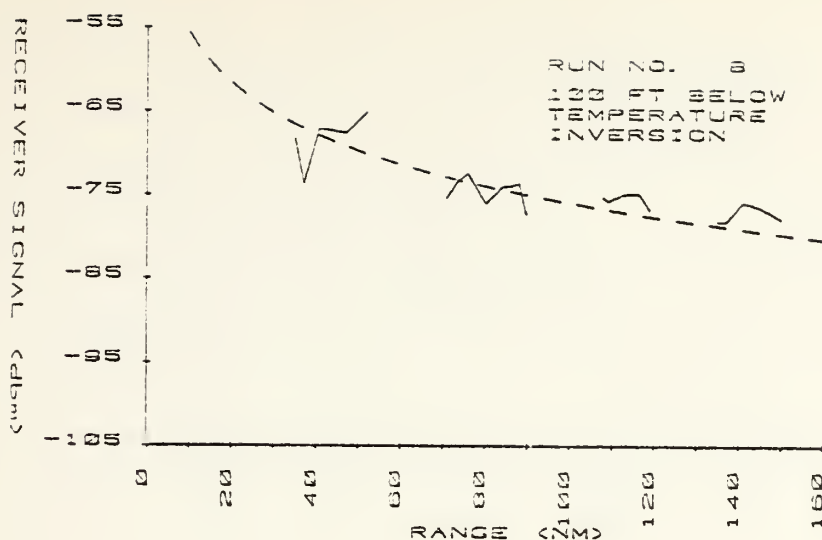


Figure 21.

Run 8 Loss Curve. Aircraft 100 ft. below temperature inversion. Dashed line is calculated free space power.

levels were the highest obtained in the duct during this experiment. Periods of no data (due to the sawtooth profile) make determination of maxima and minima impossible for this data.

Figure 22 is the loss curve for run 9. The curve does not show the high average power level of run 8. The average power level is 10 db below free space at the maximum occurring at 80 nm. The reasons for the difference in power in the duct between run 8 and run 9 is connected to the duct width and multiple duct system effects discussed above. However, the lack of recognizable period for power measurements in the duct is characteristic of other runs not exhibiting the multiple duct system of run 9.

V. CONCLUSIONS AND RECOMMENDATIONS

The purpose of this experiment was to measure received power at low altitudes during surface based ducting conditions, to compare the measurements to theoretical predictions for verification of the theory, and to study the feasibility of using the predictions to enhance the use of Navy systems. Refractive ducting conditions during this experiment were elevated and inhomogeneous with range in all cases and multilayered in some cases. This was unfortunate since, for the experimental procedure used, theoretical predictions indicate surface based duct conditions would yield the best results. As expected, ray theory and single mode approximation theory proved to be severely limited in predicting horizontal power patterns. Ray theory gives only a qualitative picture of the location of maxima and only within a duct. The single mode theory does not have the capability to predict power fluctuations in the diffraction region.

For conditions of wide, low ducts the measured received power patterns below the elevated ducts agreed qualitatively with the waveguide mode theory predictions for surface based ducts. In conditions of higher and thinner ducts, agreement with theory was not good. The interference of modes from various ducts in the multiple duct system appears to destroy

the power pattern below the ducts. The lack of capability of the waveguide mode program used here to find all significant modes limits the program's ability to predict results for the conditions of this experiment.

The results of this experiment imply that there are range dependent maxima and minima in the received power at a surface site even when the duct is elevated. This effect could be used to enhance signal reception. However, in the elevated duct conditions encountered in this experiment, use of currently available theories to predict the ranges of occurrence is not feasible, except possibly in the presence of wide, low ducts. Verification of the existence of maxima and minima at ranges beyond the horizon is significant and warrants further investigation. The ducting conditions encountered during this experiment were far from ideal for investigating this type of effect. Additional tests in surface based ducting conditions should be carried out. There currently exist more advanced techniques for waveguide solutions [Ref 23], but present theories are not adequate. New program techniques capable of accounting for nonhomogeneous M conditions are needed. Improved theoretical models and their verification by additional experiment could provide predictions that would allow tactical utilization of propagation patterns within and below refractive ducts.

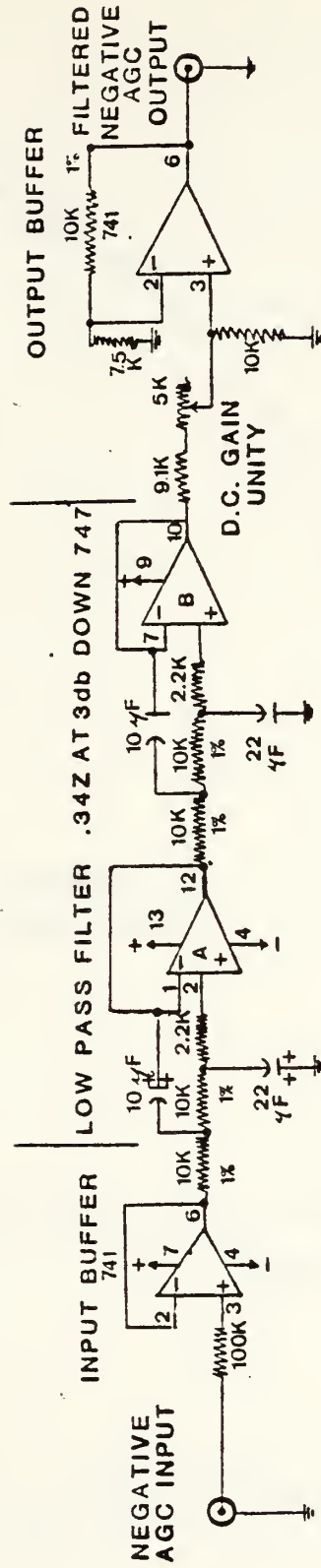


Figure A-1
Filter Schematic

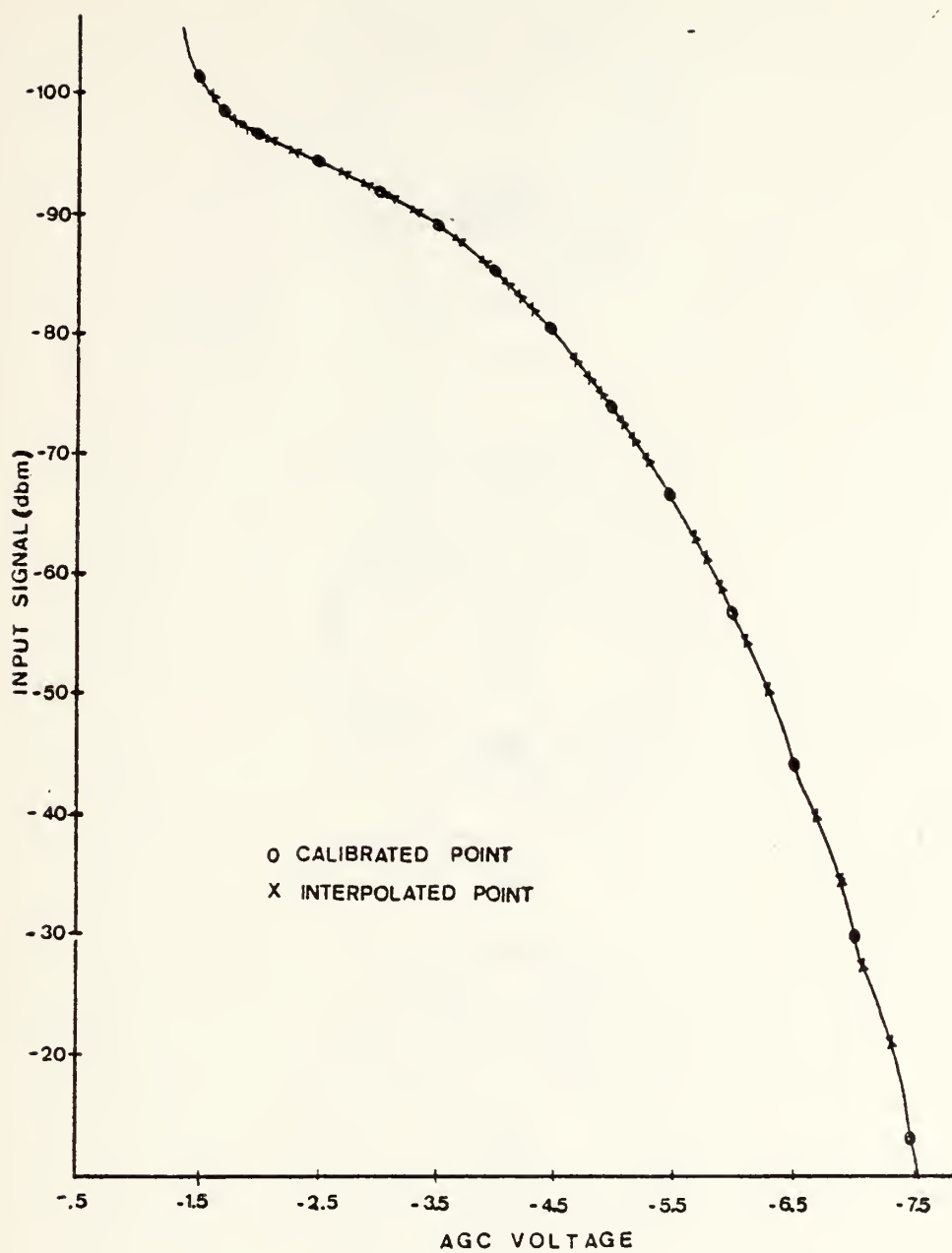
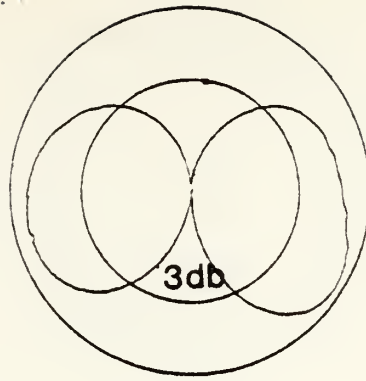
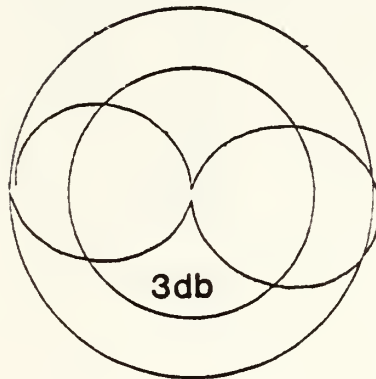


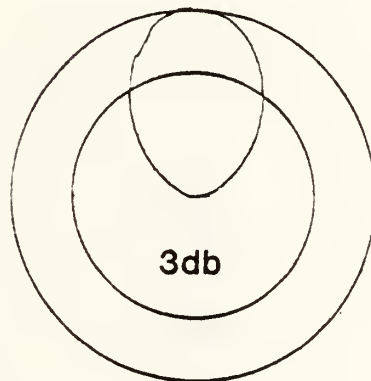
Figure A-2
AN/URR-35 Input Power versus Negative AGC Voltage



(a)

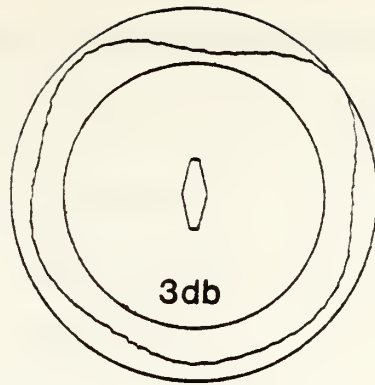


(b)

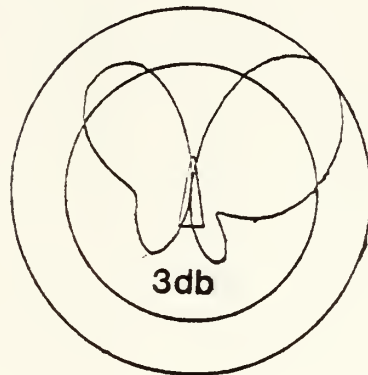


(c)

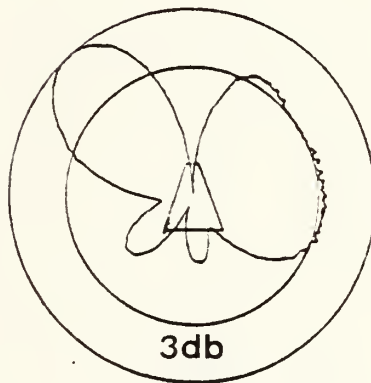
Figure A-3.
Relative Antenna Patterns (a) AN/AS 360 Monopole
(b) AN/AT 150 Dipole (c) Log Periodic with 6 db
attenuation.



(a)



(b)



(c)

Figure A-4.
Relative Antenna Patterns AN/AT 879A
(a) Horizontal (b) Vertical, short axis
(c) Vertical, long axis

TABLE A-1

COAXIAL LOSS MEASUREMENTS

Cable No.	Use	Length (ft.)	Loss (db)
1	Transmitter	3	-0.3
2	Receiver	6	-0.3
3	Receiver	35	-2.8
4	Receiver Calibration	3	-0.3

TABLE A-2

FLIGHTS AND PROFILES

FLIGHT	RUN	DATE	CONDITIONS
	1	06/03/81	U. S. S. ACANIA EQUIPMENT TEST
	2	06/10/81	U. S. S. ACANIA EQUIPMENT TEST
	3	08/07/81	U. S. S. ACANIA DUCT TEST
	4	08/10/81	U. S. S. ACANIA DUCT TEST
	5	08/12/81	U. S. S. ACANIA DUCT TEST
01	6	09/05/81	AIRCRAFT EQUIPMENT TEST
02	7	09/07/81	AIRCRAFT DUCT TEST
03	8	09/09/81	AIRCRAFT DUCT TEST
04	9	09/10/81	AIRCRAFT DUCT TEST
05	10	09/12/81	AIRCRAFT MANEUVER TEST
05	11	09/12/81	AIRCRAFT DUCT TEST
06	12	09/15/81	AIRCRAFT DUCT TEST
06	13	09/15/81	LADDER SOUNDINGS AT 10 NM.
07	14	09/16/81	LADDER SOUNDINGS AT 40 NM.
08		09/18/81	MONTEREY AREA SOUNDINGS
09	15	09/19/81	AIRCRAFT DUCT TEST
10	16	09/20/81	AIRCRAFT DUCT TEST

TABLE A-3

POWER CONVERSION COEFFICIENTS

LIMITS	NO.	COEFFICIENT
-3.0 > V > -7.5	1	0.000000000001
	2	0.000000000016
	3	-0.000000002814
	4	0.000000020084
	5	-0.00036753636
	6	-0.02466755120
	7	-0.85602769000
	8	-6.14638130000
	9	-22.04580440000
	10	-124.07521170000
-2.0 > V > -3.0	1	1.19999950000
	2	0.99999900000
	3	-100.10000000000
-1.4 > V > -2.0	1	-5.84600000000
	2	-48.17200000000
	3	-123.73800000000
	4	-198.85900000000

TABLE A-4

DUCT TOPS AND BOTTOMS

MONTEREY DATA

FLIGHT	RUN	RANGE (NM)	TOP (M)	BOTTOM (M)
3	8	8	506	180
		30	473	120
		56	546	200
		67	525	313
		92	589	399
		102	582	437
		130	650	487
		155	711	497
4	9	5	534	260
		38	461	262
		50	520	262
		149	673	495
6	12	3	547	240
		30	541	253
		40	548	400
		71	660	226
		83	652	345
		113	697	568
		123	709	537
9	15	10	310	132
		50	842	472
10	16	4	238	0
		7	565	331
		53	682	559
		129	562	426
		150	590	400

TABLE A-5

DUCT TOPS AND BOTTOMS

GUADALUPE ISLAND DATA

RANGE (NM)	TOP (M)	BOTTOM (M)
40	303	121
70	303	121
90	303	181
140	303	212

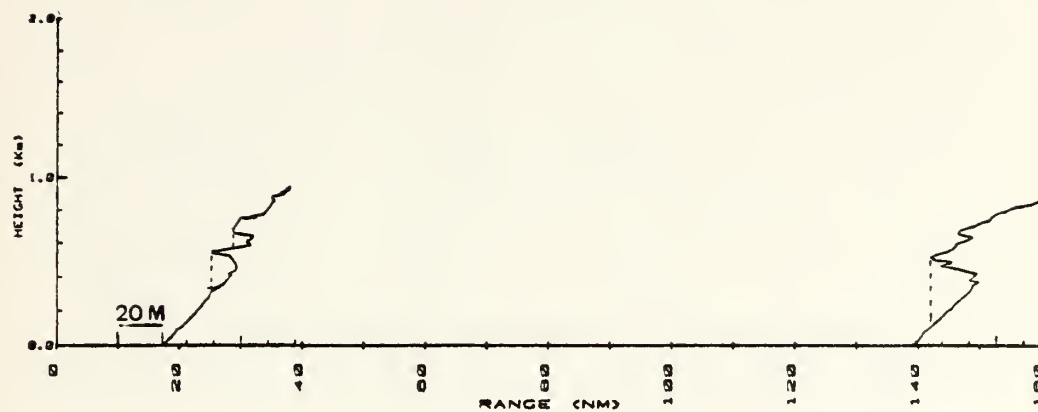
TABLE A-6

DUCT TOPS AND BOTTOMS

ROPETRICK II DATA

RANGE (NM)	TOP (M)	BOTTOM (M)
11	1636	1090
28	1575	1060
41	1575	1030
54	1393	969
65	1454	1030
97	1393	1000
132	1515	1000
167	1363	878

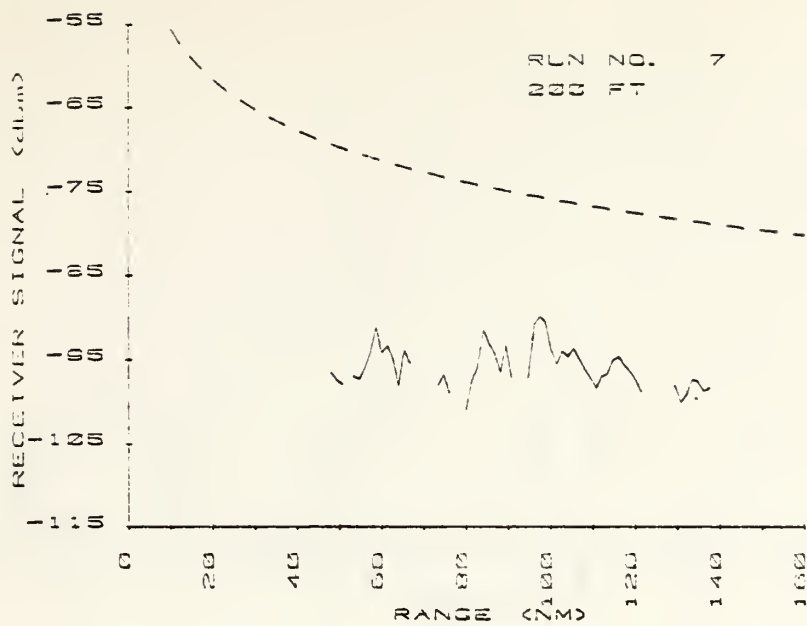
APPENDIX B



(a)

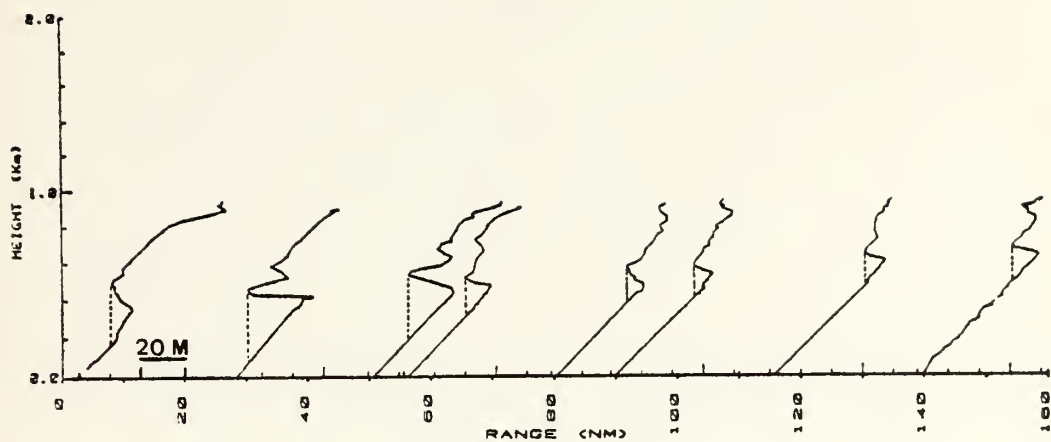
(b)

Figure B-1. Run 7 (a) M Profiles

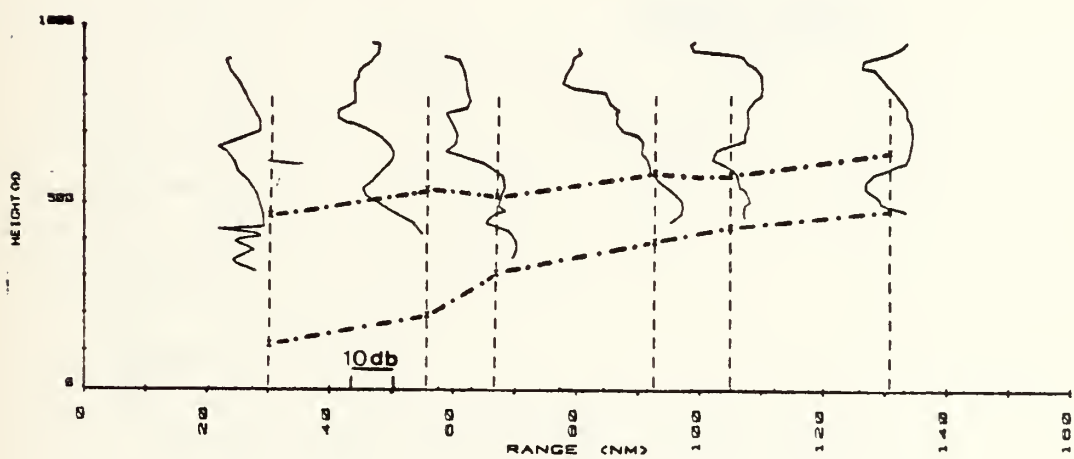


(a)

Figure B-2. Run 7. (a) 200 ft. Aircraft altitude
Dashed line is free space power



(a)

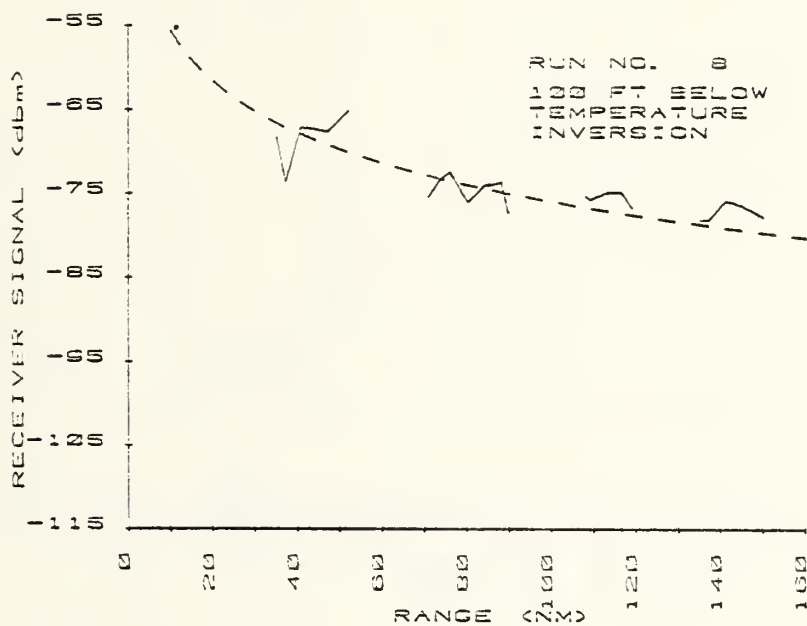


(b)

Figure B-3. Run 8 (a) M profiles (b) Height gain curves
Dashed line is free space power. Dot/dashed line connects
point measurements of duct top and duct bottom.

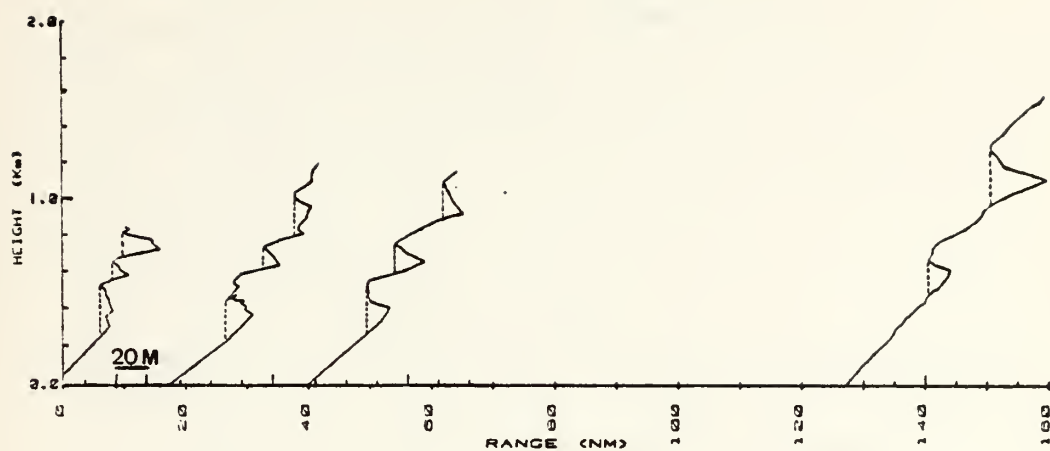


(a)

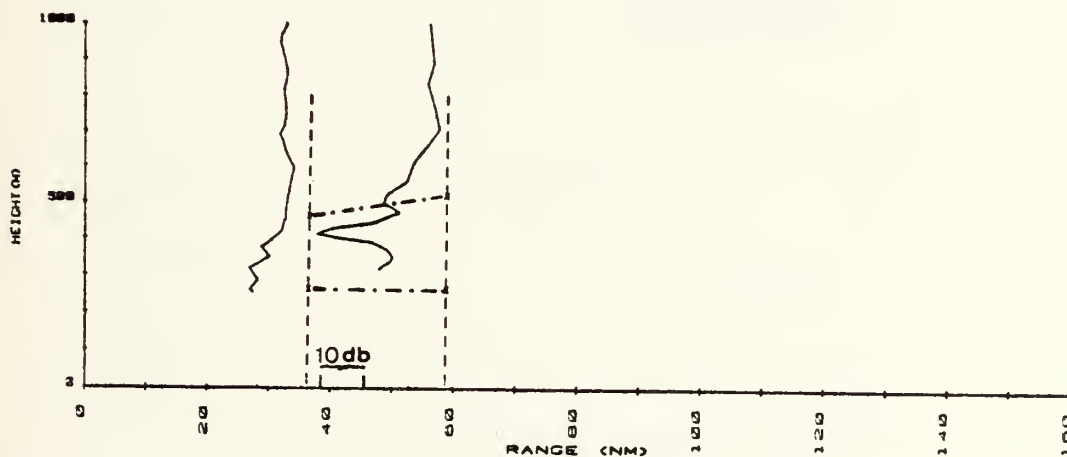


(b)

Figure B-4. Run 8 (a) 130 ft. Aircraft altitude
(b) Aircraft 100 ft. below temperature inversion
Dashed line is free space power.

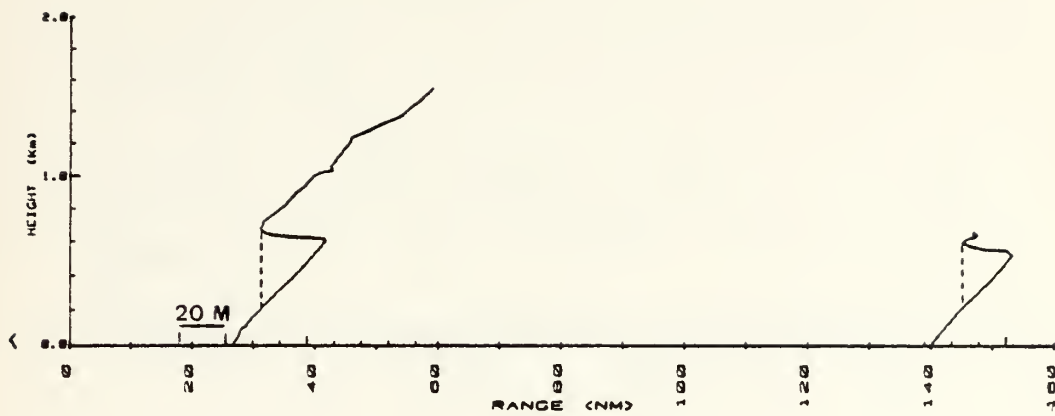


(a)



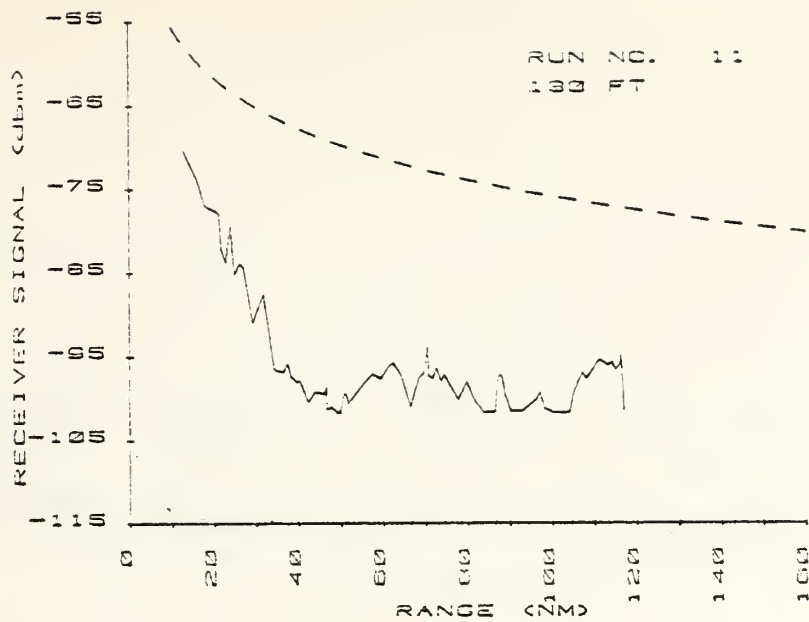
(b)

Figure B-5. Run 9 (a) M profiles (b) Height gain curves
Dashed line is free space power. Dashed/dot line connects
point measurements of duct top and duct bottom.

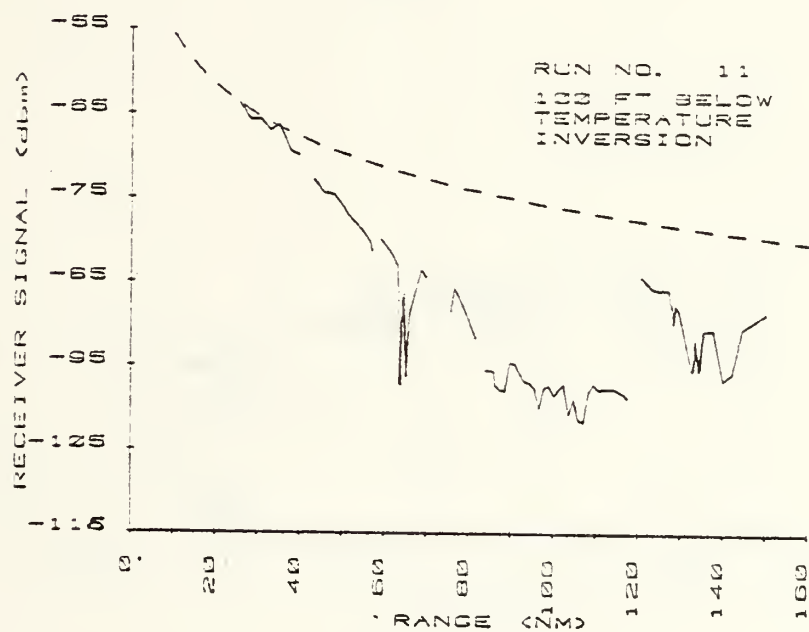


(a)

Figure B-7. Run 11 (a) M profiles

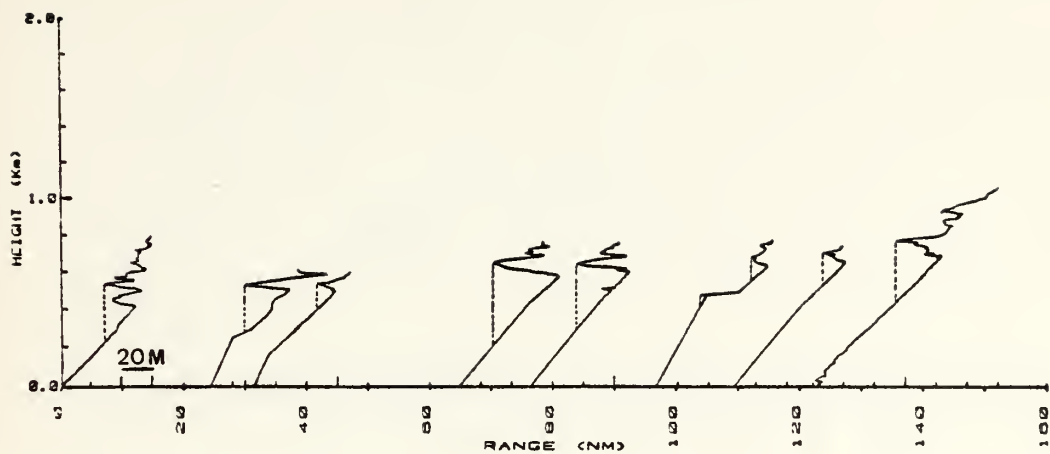


(a)

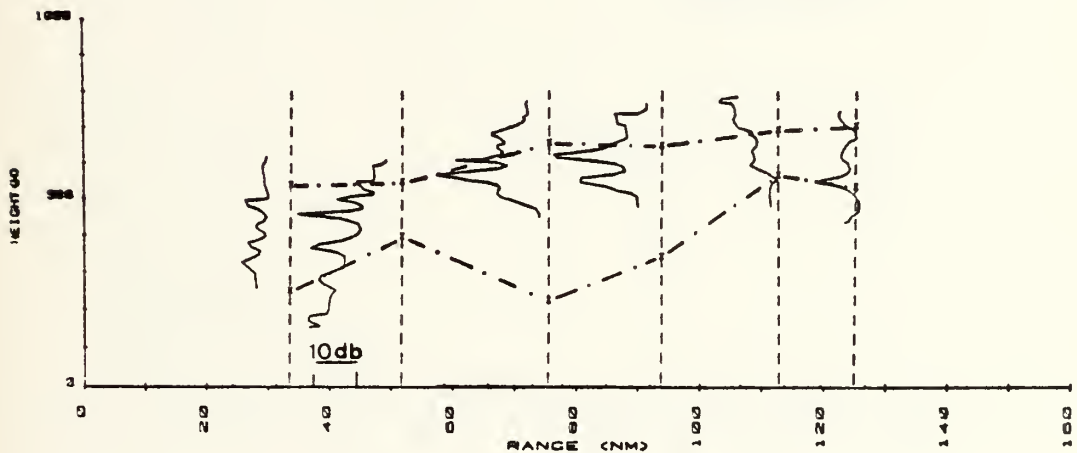


(b)

Figure B-8. Run 11 (a) Aircraft altitude 130 ft.
 (b) Aircraft 100 ft. below temperature inversion.
 Dashed line is free space power.



(a)

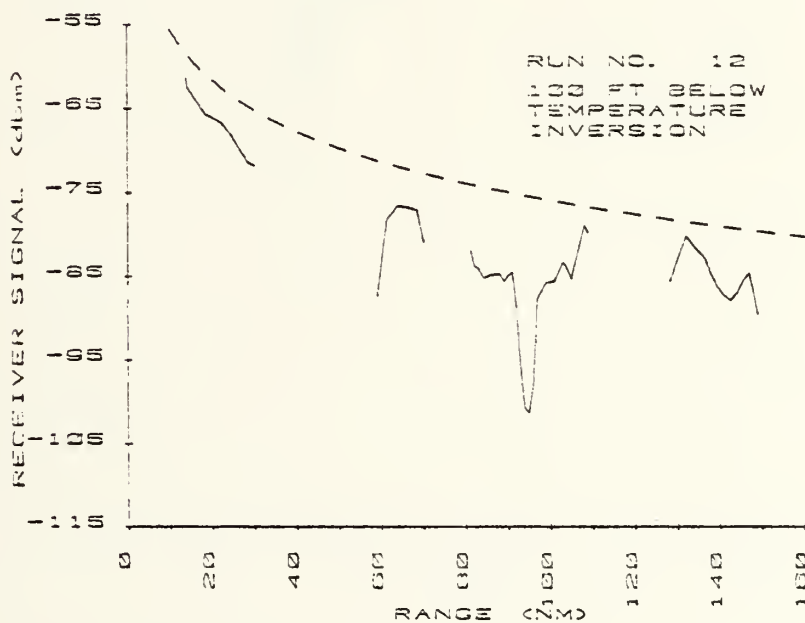


(b)

Figure B-9. Run 13 (a) M profiles (b) Height gain curves
Dashed line is free space power. Dashed/dot line connects
point measurements of duct top and duct bottom.

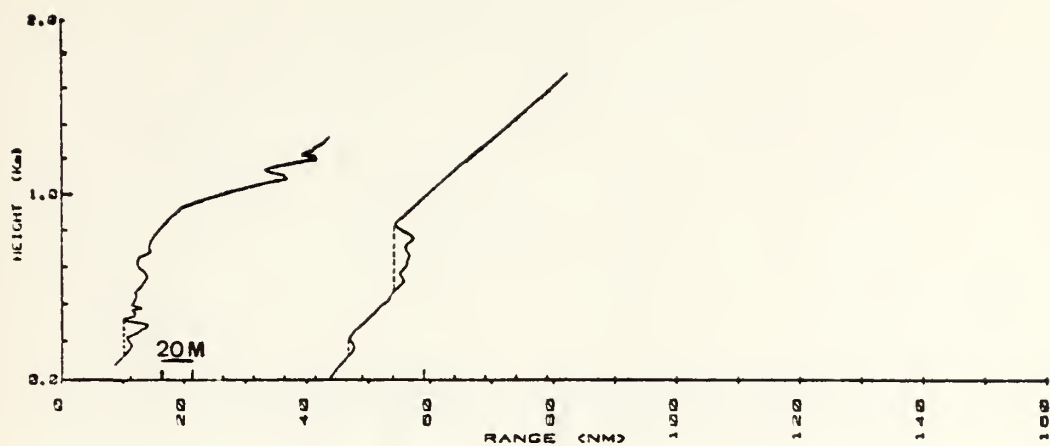


(a)



(b)

Figure B-10. Run 12 (a) Aircraft altitude 130 ft.
 (b) Aircraft 100 ft. below temperature inversion.
 Dashed line is free space power.

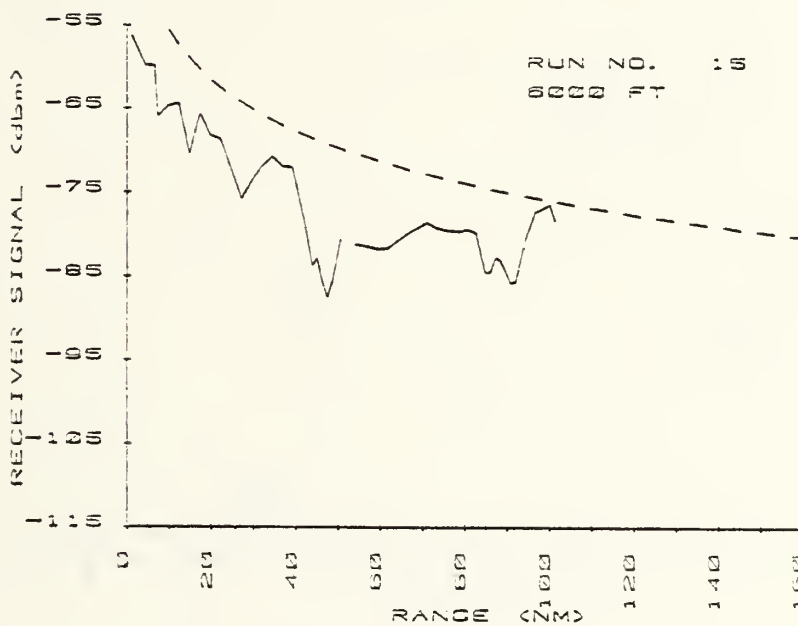


(a)

Figure B-11. Run 15 (a) M profiles

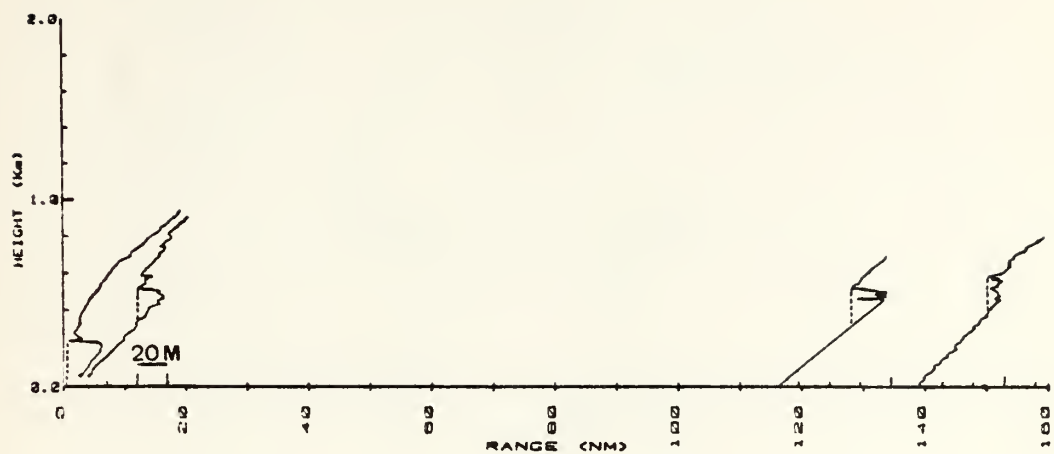


(a)

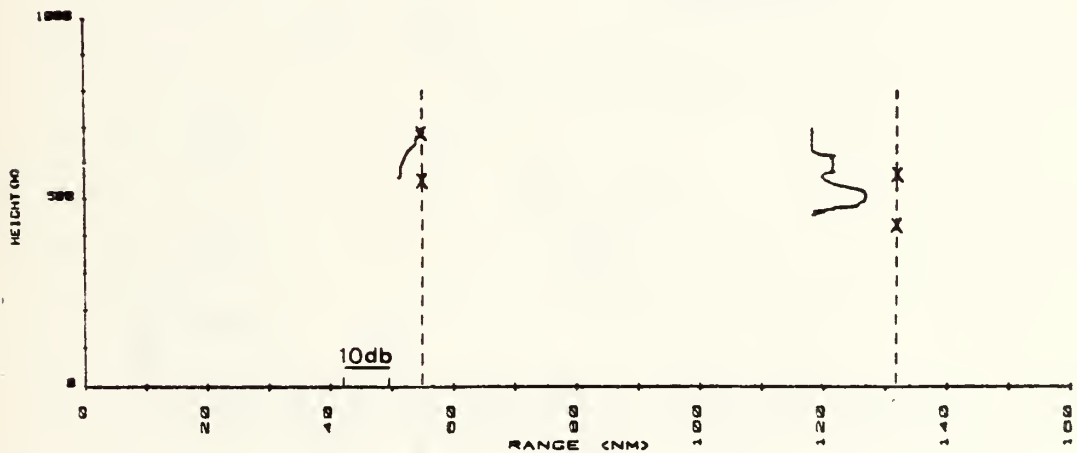


(b)

Figure B-12. Run 15 (a) Aircraft altitude 130 ft.
 (b) Aircraft altitude 6000 ft.
 Dashed line is free space power.

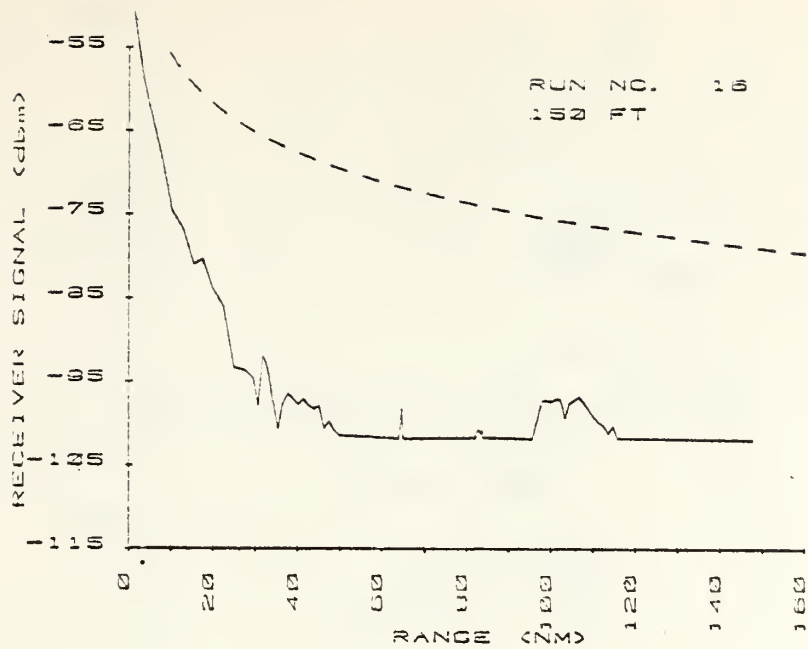


(a)

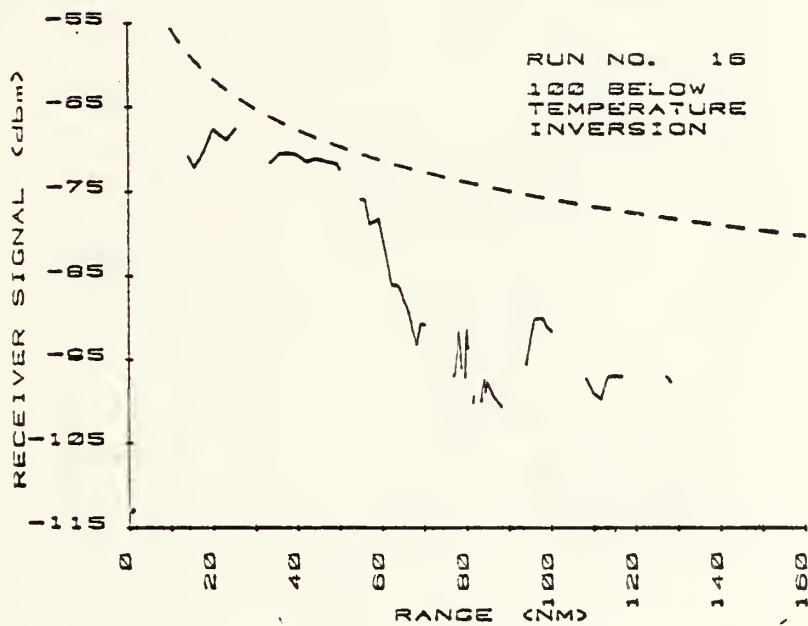


(b)

Figure B-13. Run 16 (a) M profiles (b) Height gain curves
Dashed line is free space power.
X indicates duct top and bottom.

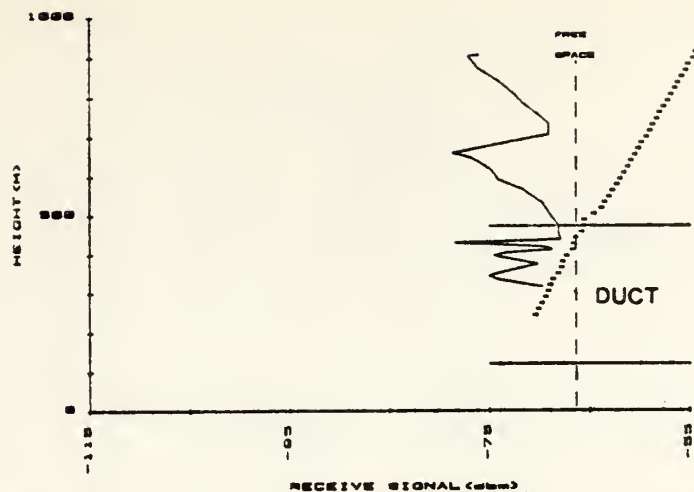


(a)

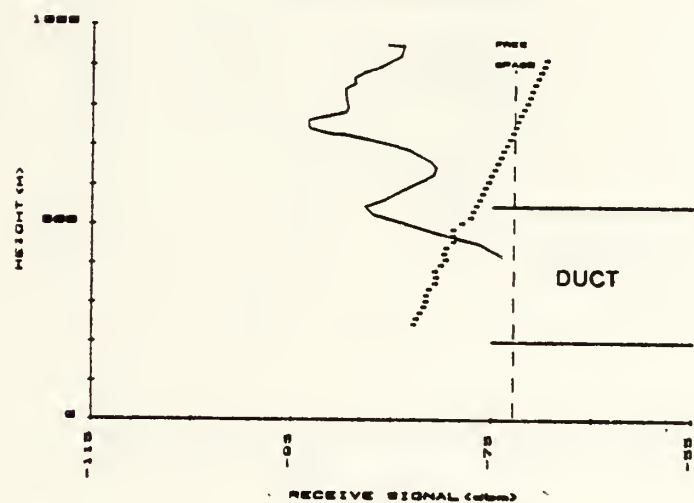


(b)

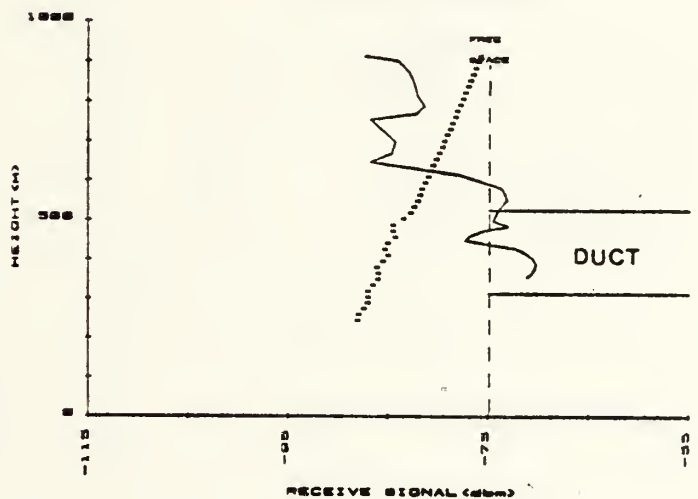
Figure B-14. Run 16 (a) Aircraft altitude 130 ft.
(b) Aircraft 100 ft. below temperature inversion.
Dashed line is free space power.



(a)

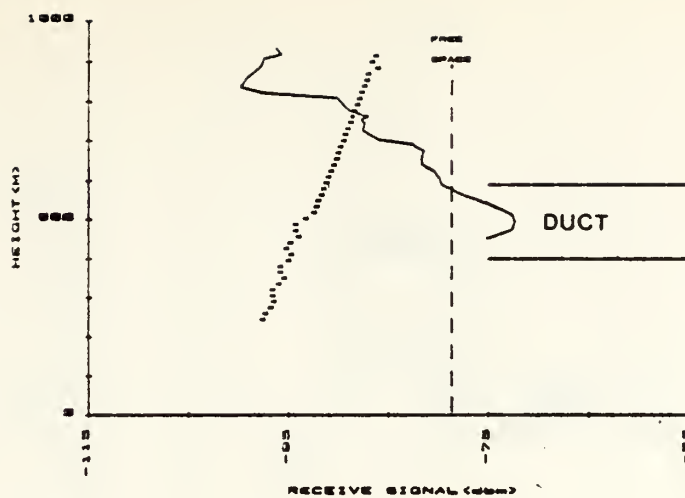


(b)

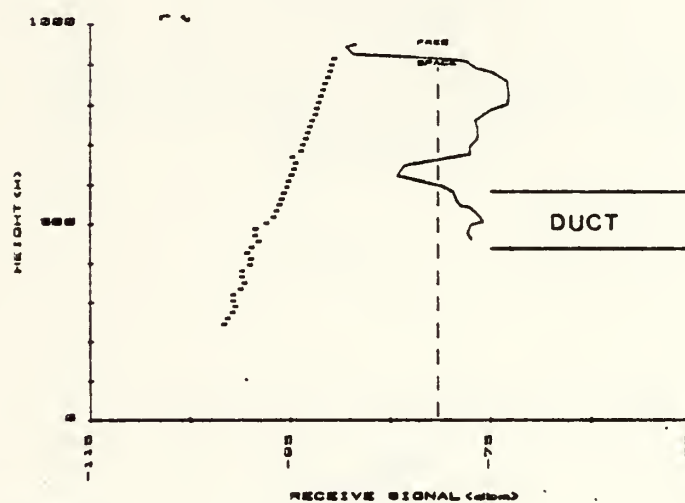


(c)

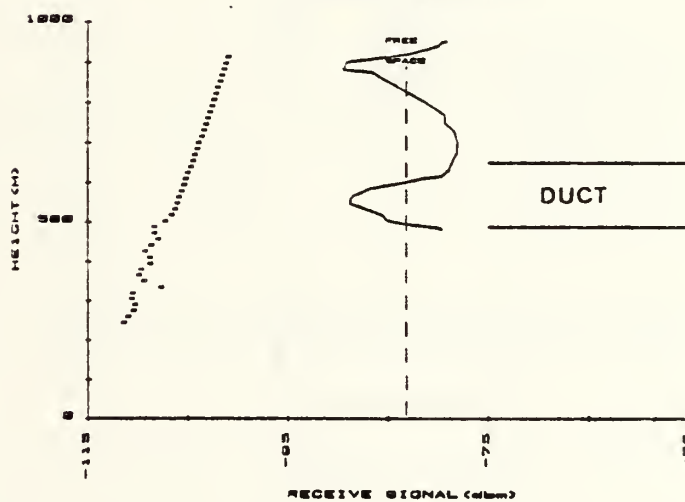
Figure B-15. Run 8 height gain curves. Power sum.
Dotted line is mode theory using 67 nm. M profile.
(a) 30 nm. (b) 56 nm. (c) 67 nm.



(a)

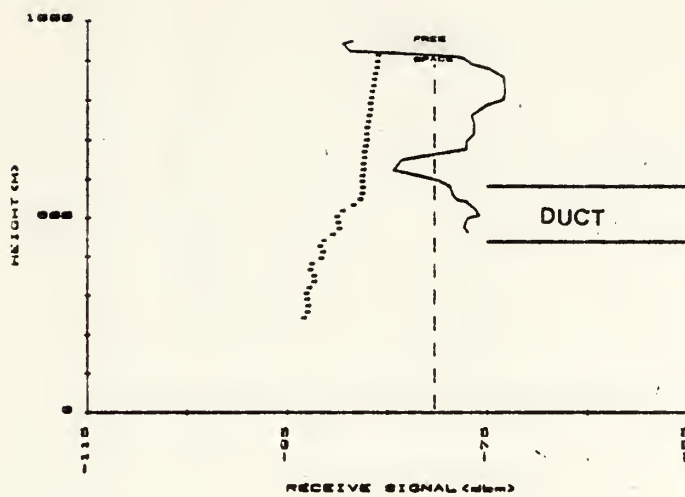


(b)

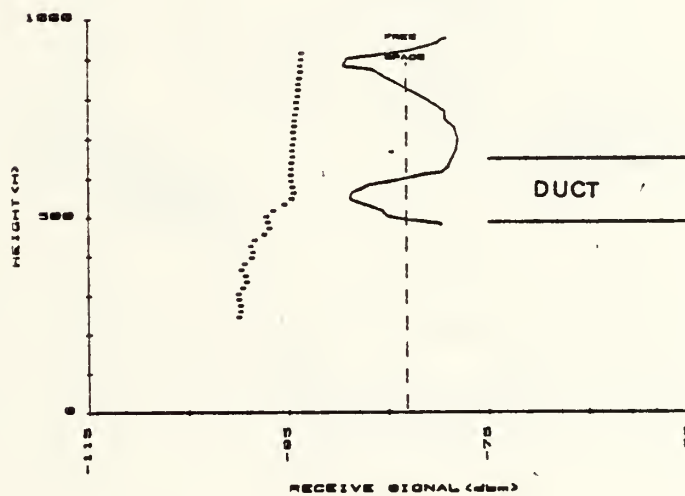


(c)

Figure B-16. Run 8 height gain curves. Power sum.
Dotted line is mode theory using 67 nm. M profile
(a) 93 nm. (b) 102 nm. (c) 131 nm.

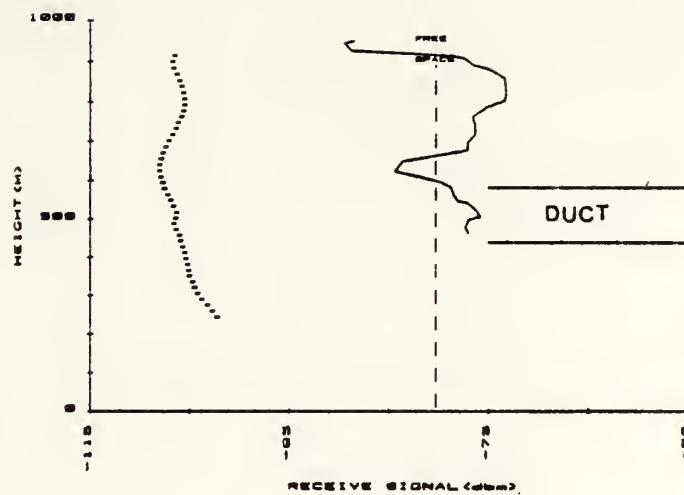


(a)

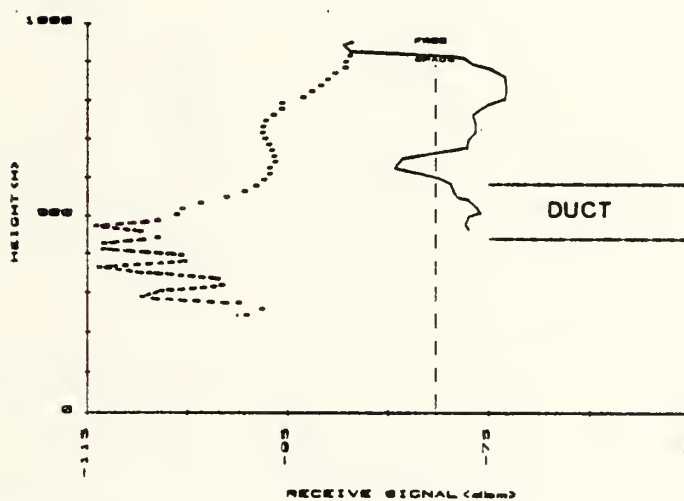


(b)

Figure B-17. Run 8 height gain curves. Power sum.
Dotted line is mode theory using 10 nm. M profile.
(a) 102 nm. (b) 131 nm.

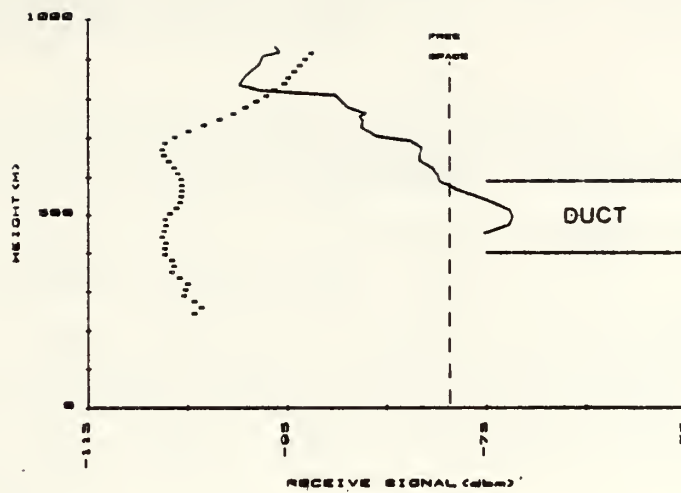


(a)

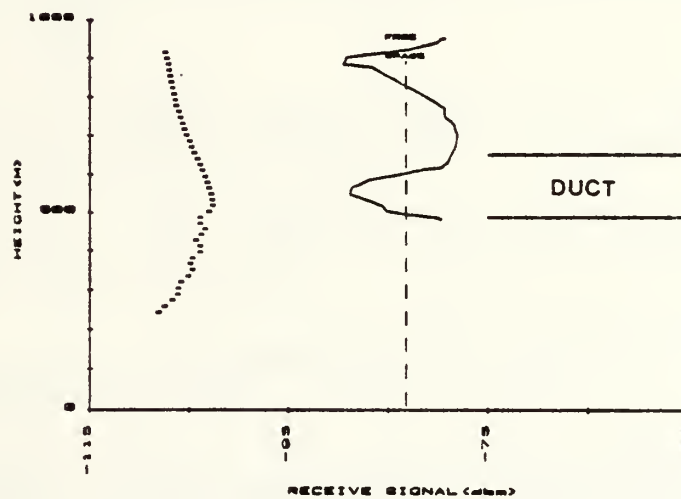


(b)

Figure B-18. Run 8. 102 nm. height gain curves.
Dotted line is mode theory. Vector sum.
(a) 67 nm. M profile. (b) 10 nm. M profile.



(a)



(b)

Figure B-19. Run 8 height gain curves. Dotted line is mode theory using 67 nm. M profile. Vector sum.
(a) 91 nm. (b) 130 nm.

LIST OF REFERENCES

1. Naval Postgraduate School Report NPS-61-80-017, Naval Postgraduate School Shipboard and Aircraft Meteorological Equipment, by G. E. Schacher, et. al., 1980.
2. Naval Electronics Systems Command Report 0967-LP-544-5010, Radio set AN/GRC-171. Operations Service and Circuit Diagrams, 1 March 1975.
3. Transco Products Inc., Microwave Antennas Catalogue 80, Description, AN/AT 879A, March 1981.
4. Bureau of Naval Ships Publication 91906, Instruction Book for Radio Receiving Set AN/URR-35B.
5. American Radio Relay League Publication No. 15, Antenna Handbook, 1970, p. 43.
6. Bean, B. R. and Dutton, E. J., Radio Meteorology, National Bureau of Standards Monograph 92, 1966.
7. Kerr, D. E., Propagation of Short Radio Waves, McGraw-Hill, N. Y., 1951.
8. Op. cit., Kerr, p. 6
9. Naval Ocean Systems Center Report TN 669, Revised FNWC Radar Propagation Model, by C. P. Hattan, May 1979.
10. Barton, I. J., "The Importance of Tilted Layers in the Tropospheric Ducting of Radio Waves Over the Timor Sea," Radio Science, v. 8, no. 8, p. 727-732, 1973.
11. Budden, K. G., The Waveguide Mode Theory of Wave Propagation, Logos, London, 1961.
12. Naval Ocean System Center Report TN 153 Application of a Root Finding Method for Tropospheric Ducting Produced by Trilinear Refractivity Profiles, by C. L. Goodhart and R. A. Pappert, September 1977.
13. Pappert, R. A. and Goodhart, C.L., "Case Studies of Beyond-the-Horizon Propagation in Tropospheric Ducting Environments," Radio Science, v. 12, Jan.-Feb., 1977.

14. Skillman, J. L. and Wood, D. R., "Experimental Study of Elevated Ducts," Proceedings of the Conference on Atmospheric Refractive Effects Assessment, J. H. Richter, ed., 1979.
15. Op. cit., Skillman, p. 103
16. Op. cit., Skillman, p. 103
17. Op. cit., Pappert
18. Op. cit., Pappert, p. 12
19. Op. cit., Budden, p. 107
20. Op. cit., Pappert, p. 76
21. Op. cit., Hattan
22. Op. cit., Hattan p. 23
23. Op. cit., Barton
24. Electromagnetic Compatibility Analysis Center Report ESD-TR-81-102, A Model to Calculate EM Fields in Tropospheric Duct Environments at Frequencies through SHF. by S. Marcus and W. D. Stuart, September, 1981.

INITIAL DISTRIBUTION LIST

	No. Copies
1. Defense Documentation Center Cameron Station Alexandria, Virginia 22314	2
2. Library, Code 0142 Naval Postgraduate School Monterey, California 93940	2
3. Dean of Research, Code 012 Naval Postgraduate School Monterey, California 93940	1
4. Professor G. E. Schacher, Code 61sq Naval Postgraduate School Monterey, California 93940	2
5. Professor J. B. Knorr, Code 62 Ko Naval Postgraduate School Monterey, California 93940	1
6. Professor K. L. Davidson, Code 63Ds Naval Postgraduate School Monterey, California 93940	1
7. Lcdr. J. C. Boudreaux 6815 Lazy Clouds Point San Diego, California 92120	1
8. Mr. Herb Hitney, Code 532 Naval Ocean System Center San Diego, California 93940	1
9. Professor J. Dyer, Code 61Dy Naval Postgraduate School Monterey, California 93940	1

The
B73
c.1

Thesis
B7335
c.1

Boudreaux

Atmospheric effects
on ultra high fre-
quency radio pro-
pagation.

OCT 20 85

197255

30005

Thesis
B7335
c.1

Boudreaux

Atmospheric effects
on ultra high fre-
quency radio pro-
pagation.

197255

thesB7335

Atmospheric effects on ultra high freque



3 2768 002 07343 9

DUDLEY KNOX LIBRARY